Geologic and geomorphic controls on rockfall hazard: how well do past rockfalls predict future distributions?

Josh Borella [1,2], Mark Quigley [3,2], Zoe Krauss [4,1], Krystina Lincoln [5,1], Januka Attanayake [3], Laura Stamp [5,1], Henry Lanman [6,1], Stephanie Levine [7,1], Sam Hampton [1,2], Darren Gravley [1,2]

[1] Frontiers Abroad, 3 Harbour View Terrace, Christchurch, 8082, New Zealand
[2] Department of Geological Sciences, University of Canterbury, Christchurch, 8041, New Zealand
[3] School of Earth Sciences, The University of Melbourne, Victoria, 3010, Australia
[4] Department of Geology, Colorado College, Colorado Springs, CO, 80903, USA
[5] Department of Geosciences, Williams College, Williamstown, MA, 01267, USA
[6] Department of Geology, Whitman College, Walla Walla, WA, 99362, USA
[7] Department of Geology, Carleton College, Northfield, MN, 55057, USA

Correspondence: Josh Borella (josh@frontiersabroad.com)

KEYWORDS: Rockfall hazard, boulder spatial distributions, frequency-volume distributions, Canterbury Earthquake Sequence, prehistoric rockfall boulders, deforestation, rockfall source characteristics, rockfall physical properties, rockfall numerical modelling, Christchurch

Abstract

To evaluate the geospatial hazard relationships between recent (contemporary) rockfalls and their prehistoric predecessors, we compare the locations, physical characteristics, and lithologies of rockfall boulders deposited during the 2010-2011 Canterbury earthquake sequence (CES) (n=185) with those deposited prior to the CES (n=1093). Population ratios of pre-CES to CES boulders at two study sites vary spatially from ~5:1 to 8.5:1. This is interpreted to reflect *(i)* variations in CES rockfall flux due to intra- and inter-event spatial differences in ground motions (e.g. directionality) and associated variations in source cliff responses, *(ii)* possible variations in the triggering mechanism(s), frequency, flux, record duration, boulder size distributions, and post-depositional mobilization of pre-CES rockfalls relative to CES rockfalls, and *(iii)* geological variations in the source cliffs of CES and pre-CES rockfalls. On interfluves, CES boulders traveled approximately 100 to 250 m further downslope than prehistoric (pre-CES) boulders, interpreted to reflect reduced resistance to CES rockfall transport due to preceding anthropogenic hillslope de-vegetation. Volcanic breccia boulders are more dimensionally equant, rounded, larger, and traveled further downslope than coherent lava boulders, illustrating clear geological control on rockfall hazard. In valley bottoms, the furthest-traveled pre-CES boulders are situated further downslope than CES boulders due to *(i)* remobilization of pre-CES boulders by post-depositional processes such as debris flows, and *(ii)* reduction of CES boulder velocities and travel distances by collisional impacts with pre-CES boulders. A considered earth-systems approach is required when using preserved distributions of rockfall deposits to predict the severity and extents of future rockfall events.

1 Introduction

Rockfall deposits pervade many mountainous and hilly regions worldwide (Varnes, 1978; Evans and Hungr, 1993; Wieczorek, 2002; Dorren, 2003; Guzzetti et al., 2003) and can provide important data for assessing future rockfall hazards (Porter and Orombelli, 1981; Keefer, 1984; Dussauge-Peisser et al., 2002; Copons and Vilaplana, 2008; Wieczorek et al., 2008; Stock et al., 2014; Borella et al., 2016a). Their characteristics (e.g. location, size, morphology) may be used to complement numerical rockfall modeling scenarios (Agliardi and Crosta, 2003; Dorren et al., 2004; Heron et al., 2014; Vick, 2015; Borella et al., 2016a) and inform engineering-design criteria for rockfall mitigation structures (e.g. impact fences, tiebacks, protection forests) (e.g. Agliardi and Crosta, 2003; Dorren et al., 2004; Guzzetti et al., 2004). However, natural and anthropogenic changes to the landscape (including changes to the rockfall source and slope areas) between successive rockfall events and the post-depositional history for rockfalls can be complex (e.g. Borella et al., 2016a,b). To better understand how past rockfalls provide suitable proxies for characterizing future hazard, comparisons between the geologic and geomorphic attributes of individual rockfall events and cumulative amalgamations of many events are valued. Critical evaluations of possible intervening changes to the landscape that may influence the mechanics of rockfall production and travel are an important component of these studies.

More than 7000 mapped individual rocks fell from cliffs in the Port Hills in southern Christchurch during the 2010-2011 Canterbury Earthquake Sequence (CES) in New Zealand's South Island (Massey et al., 2014). Most of the rockfalls (>6000) occurred during the 22 February 2011 moment magnitude (Mw) 6.2 and 13 June 2011 Mw 6.0 Christchurch earthquakes (Massey et al., 2014). Approximately 200 houses were impacted, 100 houses severely damaged, and five fatalities caused by falling rocks in the 2011 February earthquake (Massey et al., 2014; Grant et al., 2018). CES rockfalls were characterized by boulder-size distribution, runout distance (the distance a rock travels down a slope from its source), source-area dimensions, and boulder-production rates over a range of triggering peak ground accelerations (Massey et al., 2012a-e, 2014, 2017; Quigley and Mackey, 2014; Quigley et al., 2016).

Subsequent field investigations revealed an abundance of pre-CES rockfall deposits in CES rockfall areas (Townsend and Rosser, 2012; Mackey and Quigley, 2014; Borella et al.,

2016a,b), suggesting multiple rockfall events had occurred at these sites in the past (Mackey and Quigley, 2014; Borella et al., 2016a,b; Sohbati et al., 2016). Retrospectively, these pre-CES deposits had potential value to contribute to hazard assessments during land-planning and urban development in Christchurch prior to the CES; however, there is no evidence that they did so (Townsend and Rosser, 2012; Litchfield et al., 2016). At one well-studied location (Rapaki) in the Port Hills of southern Christchurch, CES and pre-CES boulder populations were shown to have similar volumetric size and morphology characteristics, but a significant population of CES boulders had longer maximum runout distances than their pre-CES counterparts (Borella et al., 2016a). Pre-CES rockfalls were dated using independent approaches to >3-15 ka (Mackey and Quigley, 2014; Sohbati et al., 2016; Borella et al., 2016b). With the aid of numerical modeling of rockfall trajectories (using RAMMS - rapid mass movement simulation) these data were collectively interpreted to suggest that anthropogenic deforestation between pre-CES and CES rockfalls was the primary cause for the observed spatial distinctions in CES and pre-CES rockfall distributions (Borella et al., 2016a). Elsewhere in the Port Hills and greater Banks Peninsula, the causes for differences in the spatial distribution between CES and pre-CES rockfalls are less clear and in some locations the current positions of pre-CES boulders extend further distances from source cliffs than their CES counterparts. A more integrated and regional understanding of the geologic, geomorphic, seismogenic, and anthropogenic controls on rockfall distributions has the potential to inform rockfall hazard analyses for land-zoning and engineering considerations here and elsewhere (e.g. Lan et al., 2010).

In this study we document the location, volume, morphology, and lithology for individual (n=1093) pre-CES rockfall boulders at two sites (Rapaki and Purau) in the Banks Peninsula near Christchurch, New Zealand. The spatial distributions and physical attributes for pre-CES boulders are compared to rockfall boulders (n=185) deposited at the same sites during the 2010-2011 CES. RAMMS bare-earth and forested numerical modelling scenarios are conducted to help evaluate the influence of natural and anthropogenic factors on rockfall distributions, identify boulder sub-populations that have likely experienced post-emplacement mobility, determine the relative timing of pre-existing rockfalls (i.e. prehistoric or historic), and evaluate the efficacy of RAMMS in replicating empirical CES and prehistoric boulder spatial distributions. We highlight the complexity of interpreting future rockfall hazard based on former boulder distributions (particularly location) due to: (i) potential landscape changes including deforestation, (ii) changes in rockfall source (e.g. progressive emergence of bedrock

sources from beneath sedimentary cover), (iii) remobilization of prior rockfalls by surface processes including debris flows (primarily in channels), (iv) lithological variability effects on the type of material liberated in successive events, (v) collisional impedance with pre-existing boulders (particularly in channels/valleys), and (vi) variations in the location, size, and strong ground motion characteristics of past rockfall-triggering earthquakes and their impact on rockfall flux and boulder mobility. We use an integrated earth-systems approach, which combines a consideration of geologic, geomorphic, seismogenic, and anthropogenic influences on rockfall distributions with high-quality field-based (i.e. prehistoric and contemporary rockfall data sets) and instrumentally-recorded (seismic) data sets, and numerical modeling. Our results have broad implications for using rockfall distributions to forecast future rockfall hazard.

2 Geologic Setting

2.1 Overview

Banks Peninsula, located on the east coast of New Zealand's South Island, is comprised of three main volcanoes (Lyttelton, Akaroa, and Mt. Herbert) active between 11.0 and 5.8 Ma (Hampton and Cole, 2009) (Fig. 1). The two study sites (Rapaki and Purau) are located within the inner crater rim of the Lyttelton Volcanic complex (Figs. 1, 2, 3), the oldest of the volcanic centers and thought to be active from 11.0 to 9.7 Ma (Hampton and Cole, 2009). Source rock at both sites is classified by Sewell (1988) and Sewell et al. (1992) as part of the Lyttelton Volcanic Group (LVG) and consists of basaltic to trachytic lava flows interbedded with breccia and tuff (Mvl). Numerous dikes and minor domes are observed within the LVG. Our field observations support the reported lithologic descriptions for the two study locales. The inferred strike and dip for lava flows nearest to the study sites indicates a shallow inclination in a predominantly northerly direction for measurements nearest the Rapaki and Purau study sites (Hampton and Cole, 2009). Sewell et al. (1992) reports a similar shallow northerly to northwesterly dip of 12° for lava flows nearest Rapaki. The study areas were selected because both have abundant pre-CES and CES rockfall boulders (Fig. 4) derived from lithologically equivalent volcanic source rocks. Rapaki represents a case study location proximal to the source of the 2011 February and June Christchurch earthquakes (epicenters ~2.5-5.0 km; hypocenters ~ 5.6-7.0 km), while Purau is located more distally (epicenters ~6.6-8.4 km; hypocenters ~8.9-10.3 km). Estimated rockfall-generating peak horizontal ground velocities

(PGV) at the Rapaki site in the February and June earthquakes were ≥ 30 cm s^{-2} (Mackey and Quigley, 2014).

2.2 Rapaki study site

The Rapaki study site is situated in the Port Hills of southern Christchurch (Figs. 1, 2) on the southeastern slope of Mount Rapaki (*Te Poho o Tamatea*), which has a summit height of ~400 meters. The study hillslope is slightly concave to planar with a total area of ~0.21 km^2 and faces to the east-southeast. The source zone consists of steep to subvertical bedrock cliffs composed of stratified basaltic lava and indurated auto-breccia or pyroclastic flow deposits (Fig. 5A-C). Breccia layers are thicker (~3-10 meters) and jointing is more widely spaced (often >10 m). Coherent lava layers are comparably thin (<3 meters) and joints are more closely spaced (generally <1-2 meter). Total height and length of the source rock are ~60 meters and ~300 meters, respectively (Fig. 5A). Below the source area, is a ~23°, grassy hillslope composed of windblown sediment deposits (loess), loess and volcanic colluvium, and overlying rockfall boulders (both CES and pre-CES) (Bell and Trangmar, 1987). Rapaki village (estimated population=100 residents) lies at the hillslope base at elevations of ~70 meters (asl) to sea level (Fig. 2A,B). Anthropogenic deforestation has exposed a hillslope that is currently experiencing accelerated erosion (Borella et al., 2016a,b) in the form of mass wasting and tunnel gully formation. Shallow landslides, including debris and earth flows, are most prevalent in upper to mid-slope positions, while rill and gulley erosion predominate in lower slope positions. Rockfall is a dominant surface feature at the Rapaki study site (Mackey and Quigley, 2014; Vick, 2015; Borella et al., 2016a,b). Pre-CES and CES rockfall boulders at the study site are divided into two dominant lithology types: volcanic breccia (VB) and coherent lava (CL) basalt. During the 22 February and 13 June 2011 earthquakes, more than 650 individual CES boulders ranging in diameter from <15 cm to >3m were dislodged from the volcanic source rock near the top of Mount Rapaki, many impacting and destroying residential homes (Massey et al., 2014; Mackey and Quigley, 2014).

2.3 Purau study site

Purau is located on the southern side of Lyttelton Harbour, approximately 5 kilometers southeast of Rapaki (Figs. 1, 3). Slopes at Purau have a west-northwest aspect, the opposite of the Rapaki study hillslope. Mapping of pre-CES and CES rockfall was performed on and within

several interfluves (spurs) and bounding valleys, respectively (Fig. 3) and encompassed a total area of ~1.4 km^2. The source rock geology at Purau, including lithology and structure, is equivalent to that observed at Rapaki (Fig. 5D,E). The ridgeline (i.e. volcanic source rock) to the east obtains a maximum elevation of ~440 meters. Locally, individual vertical to subvertical bluff faces are estimated to be ~20-30 meters in height. From the base of the volcanic source rock, slopes extend downward toward Purau Bay at angles ranging from ~30° to ~5° near Camp Bay Road (Fig. 3). Field observations indicate the volcanic rock is overlain by loess, loess- and volcanic-colluvium, and pre-CES and CES rockfall boulders of small (e.g. <1 m^3) to extremely large size (e.g. >100 m^3). Deforestation of Purau slopes has left the hillside covered primarily in low-lying grass and bush. Shallow slips are abundant and are commonly observed on steep slopes, including valley flanks. Maximum landslide depth is typically ~1-1.5 meters and often exposes volcanic bedrock at bottom, indicating the overlying sediment is relatively thin. Tunnel gulley erosion predominates on canyon flanks and at lower elevations.

3 Methods

3.1 Field mapping and characterization of CES and pre-CES rockfall boulders

We mapped 1276 individual rockfall boulders at the Rapaki (pre-CES=408; CES=48) and Purau (pre-CES=684; CES=136) study sites for boulder volume ≥1.0 m^3 (see Supplementary Data, Tables S1-S4, doi:10.5061/dryad.9km1t86). Where safety conditions permitted, pre-CES and CES rockfall boulders were mapped to the base of the volcanic source rock. Location (latitude/longitude) and elevation (meters above sea level) were recorded for each rockfall deposit using a hand-held Garmin GPSMap 62s device. Boulder dimensions (i.e. height, length, width) were tape measured in the field. For pre-CES boulders partially buried to the degree that only two dimensions were adequately measurable, the shorter of the two measured lengths was used for the 3rd dimension, thus insuring a conservative boulder size estimate. No rounding factor was applied to volumetric estimations of pre-CES boulders. The lithology type was determined for each pre-CES boulder and was based primarily upon the observed dominant rock 'texture'. Boulder lithologies were categorized as VB or CL. Transitional lithologies were rarely observed (<1% of total) and assigned as VB or CL based on the volumetrically predominant rock type.

3.2 Boulder runout distance

Boulder runout distance was determined by measuring the shortest horizontal and ground-length distances, perpendicular to slope contour lines, from the nearest potential bedrock source areas to mapped boulder locations using Google Earth Professional (see Supplementary Data, Tables S5-S8, doi:10.5061/dryad.9km1t86). Runout distance was calculated for 409 pre-CES boulders and 48 CES boulders (for volume ≥ 1.0 m^3) at Rapaki. Due to safety concerns we were unable to record locations for pre-CES boulders within ~100 meters (map-length) of the volcanic source rock at this site. However, boulder frequency counts (for boulder volume ≥ 0.1 m^3) were field measured within a 300 m^2 area at distances of 0-10 meters (n=31), 30-40 meters (n=35), 60-70 meters (n=77), and 100-110 (n=24) meters from the volcanic source rock (see Appendix 1, Fig. A1). The boulder frequency counts at these distances were used to extrapolate the number of boulders across remaining sections of the study site, consistent with visual inspection of air photos. At Purau, four separate geomorphic domains (PD1-PD4) were created to evaluate pre-CES and CES boulder runout distance (see Fig. 3; Supplementary Tables S7, S8, doi:10.5061/dryad.9km1t86). The domains include interfluve and valley morphologies and target areas with both CES and pre-CES rockfall boulders, and cases where the pre-CES rockfalls were sourced from a single or limited number of rock exposures. We generally report map-length runout distance within this paper.

We used the empirical shadow angle method (Lied, 1977; Evans and Hungr, 1993) to analyze the travel distance of rockfalls at Rapaki and Purau. The shadow angle is the arctangent of the relationship Ht/Lt, where Ht is the height of fall on the talus slope (elevation difference between the apex of the talus slope and final emplacement location of the rockfall block) and Lt is the travel distance on the talus slope (horizontal distance between the apex of the talus slope and the final emplacement location of the rockfall block) (see Copons, 2009; Lied, 1977; Evans and Hungr, 1993) (see Appendix 1, Fig. A2). The shadow angle method is most suitable for our study (compared to the reach or 'Fahrboschung' angle) because it does not require identifying the source release location for individual rockfall blocks, a parameter we are unable determine for the pre-CES and CES rockfalls.

3.3 RAMMS rockfall modeling

Three model scenarios were conducted using the Rapid Mass Movements System (RAMMS) software (Bartelt et al., 2013; Leine et al., 2014). RAMMS_1 represents a bare-earth CES model and was performed to test the reliability of RAMMS in replicating the spatial distribution for CES rockfalls at Purau. RAMMS_2 assumes a vegetated slope and simulates hillslope conditions prior to deforestation (i.e. prehistoric). RAMMS_3 models the potential future rockfall hazard at Purau and assumes a bare-earth (deforested) hillslope and dry soil moisture conditions to insure a worst-case (conservative) outcome. Please see Supp. Information for more detail on the individual RAMMS modeling scenarios.

The Purau terrain was modelled using a 4-m DEM (digital elevation model) derived from LIDAR (light detection and ranging) surveys to model CES (bare-earth scenario) and pre-CES (prehistoric forested slope scenario) rockfall distributions. The rockfall boulders were modelled as rigid polyhedral. The source areas (i.e. volcanic rock) and remaining runout terrain types (i.e. loess and loess/volcanic colluvium) (Appendix 2, Table A1 and Figs. A1-A3) for the RAMMS model scenarios (i.e. RAMMS_1, _2, _3) were chosen following the methods of Vick (2015) and Borella et al. (2016a) and delineated as polygon (Appendix 2, Fig. A1) and polyline (Appendix 2, Figs. A2, A3) shapefiles in ArcGIS from field observations, desktop study of orthophotography, and satellite imagery.

Boulder shape and size are highly influential in the dynamics and runout of a rockfall event (e.g. Leine et al., 2014; Latham et al., 2008). Boulder shapes and sizes used in the model simulations were representative of the true boulder geometries observed at Purau and Rapaki (Borella et al., 2016a). Rocks shapes were created using the RAMMS 'rock builder' tool, which creates boulder point clouds based on a user-defined shape and size. All boulder shapes reflected 'real' rock bodies that have been field-scanned. For each size class of boulder, varying shapes were selected, which are simplified to equant, flat, and long. Please see Supp. Information for more detail on boulder shape and size distributions utilized in each of the RAMMS modeling scenarios.

Vegetation was modelled in RAMMS as forest drag, a resisting force acting on the rock's center of mass when located below the drag layer height. The forest was parameterized by a drag coefficient, effective up to the input height of the vegetation layer. Typical values for the drag coefficient range between 100 and 10,000 kg/s (Bartelt et al., 2013; Leine et al., 2014). Vegetation was assigned an effective height of 10 m. A variable forest density was applied to

account for the presumed denser vegetation (on average) within drainage valleys at the Purau study site (Appendix 2, Fig. A4). We assume more surface and subsurface water would be focused into topographic lows and would therefore promote denser tree growth. Within drainage valleys a uniform drag force of 6000 kg/s was applied to each of the simulated boulders. Elsewhere at the study site, a drag force of 3000 kg/s was applied. These forest values are equivalent to those utilized in Borella et al. (2016a) at Rapaki in the Port Hills of southern Christchurch. We also simulated a uniform forest density increase of 10000 kg/s (see Results). As evidenced by modern native forest analogs, tree growth was extended upward to the base of the source rock and was also applied to areas between outcropping volcanic source rock.

3.4 Strong ground motions near rockfall source cliffs

Strong ground motion accelerograms for stations LPCC, D13C, D15C, and GODS were obtained from GeoNet (www.geonet.org.nz/, Fig. 6) to analyze the influence of ground motion on rockfalls. All these stations are Kinematrics Etna instruments except LPCC, which is a CUSP-3 instrument. LPCC recorded both Mw 6.2 event on 2011-02-22 and Mw 6 event on 2011-06-13. The other stations were installed following the Mw 6.2 earthquake and thus recorded only the Mw 6 earthquake. The data were sampled at 0.005 s (Nyquist frequency 100 Hz) and filtered with an effective passband having corners ~0.05 Hz and ~40 Hz. We integrated accelerograms to produce velocity seismograms and computed envelopes using ENV = sqrt[x(t)^2 + H(x(t))^2], where x(t) are time points in the seismogram and H is the Hilbert transform. The particle velocity hodograms are calculated in the horizontal plane by rotating the horizontal orthogonal components of the seismogram to a standard N-S E-W coordinate system. The time window of particle velocity hodograms is ± 5 s around the peak of the envelope of the east component. This ensures that the most significant ground motion resulting from both phase and group velocity peaks is accurately captured. Following a similar procedure, we computed particle motion hodograms by integrating accelerograms twice. These are given in Fig. 7 (A-E). Additional methods were used to analyze D13C data following interpretation of initial results; these are described in section 5.7.

4 Results

4.1 Rockfall mapping and boulder frequencies

4.1.1 Rapaki

A comparison of the spatial distributions for pre-CES and CES rockfalls at Rapaki (Fig. 2) indicates that pre-CES rockfalls are more concentrated near the source area and have shorter maximum runout distances (560±15 m) than the furthest travelled CES rockfalls (700±15 m), that impacted Rapaki village during the 2011 Christchurch earthquakes. The CES rockfalls represent a subset of the pre-CES rockfall data set; the ratio of pre-CES (n=409) to CES (n=49) rockfalls at Rapaki is ~8.5:1 (Fig. 2). The pre-CES and CES rockfall data sets are separated into VB and CL boulders (Fig. 2, 4) to understand the influence of volcanic lithology on rockfall runout and final resting location. Very few CL boulders with volume ≥1.0 m^3 exist for pre-CES (n=18) and CES (n=3) rockfalls at Rapaki. Pre-CES and CES VB boulders display longer average and maximum runout distances than their CL counterparts (Fig. 2), and CES CL and VB boulders display longer average and maximum runout distances compared with their pre-CES equivalents. The ratio of pre-CES VB to CL and CES VB to CL rockfall boulders is ~22:1 and ~15:1, respectively (Fig. 2).

4.1.2 Purau

Pre-CES and CES rockfalls are widely distributed at the Purau study location (Fig. 3). Rockfall boulders are deposited on interfluves but are predominantly concentrated within nearby canyons, highlighting the strong influence of topography at the site (Fig. 3). Seven (7) CES detachment zones were identified in the field. CES rockfall boulders nearest to the Purau village display the longest runout distance (372 m) and most distinct spatial contrast with similarly sourced pre-CES boulders (deposited within ~105 meters of the local volcanic source rock) (Fig. 3A). Elsewhere, pre-CES boulders can be observed at further distances from the source rock than CES rockfalls. The ratio of pre-CES to CES rockfall boulders is ~5:1 (Fig. 3A). Pre-CES VB boulders are deposited throughout the Purau location, while the deposition of CL pre-CES boulders is concentrated within the central and southern drainage canyons (Fig. 6A). The ratio of pre-CES VB to CL boulders is ~2:1 (Fig. 3B). CES VB boulders (n=127) significantly outnumber CL boulders (n=9) at the Purau site (Fig. 3C), reflecting the lack of detachment within CL source rock lithologies during the CES. The ratio of CES VB to CL rockfall boulders is ~14:1 and represents a significance difference compared with the corresponding pre-CES VB:CL ratio (Fig. 3C).

4.2 Boulder morphology and other characteristics

VB boulders (Fig. 4A-F) contain small to large porphyritic volcanic clasts that exhibit minor to moderate vesicularity (up to ~10%) and are embedded within a finer crystalline and ash-bearing matrix (see Fig. 4A,C,D,F). They are dominated by equant (all axes equal length) shapes (see Fig.4C) although elongate (two short axes, one long) forms are observed. Flat (one short, two long axes) morphologies are rare. VB pre-CES boulder surfaces show a high degree of weathering and surface roughness (Fig. 4A-D,F). The surface roughness results from in-situ differential weathering between the finer crystalline host matrix and more resistant embedded volcanic clasts (see Fig. 4D). Surfaces show deep pitting, with amplitudes often exceeding 5-10 centimeters in height. CL boulders (Fig. 4G-K) are more texturally homogenous, contain fewer vesicles (estimated ~<1%) and exhibit a higher relative density (Carey et al., 2014; Mukhtar, 2014). The pre-CES CL boulder surfaces exhibit low surface roughness (i.e. smooth compared with VB boulders). Elongate and flat boulder morphologies predominate for CL boulder lithologies (Fig. 4G-K).

Both VB and CL pre-CES boulders can be observed partially to nearly completely buried by loess-colluvium (see Fig. 4A,B,G). Instances do occur, however, where no sediment is built-up at the boulder backside (Fig. 4C) due to erosion (including tunnel gully formation). Burial in hillslope sediment is most common for boulders located on midslope and footslope positions, rather than those located on upper slope elevations, where erosion dominates. Pre-CES boulders located in drainage canyons are subject to rapid deposition and erosion, and therefore can be found without any sediment pile-up or preserving large colluvial wedges. VB boulders preserve the thickest colluvial wedge sediments (see Fig. 4B).

4.3 Source rock characteristics

The volcanic source rock at Rapaki (Fig. 5A-C) and Purau (Fig. 5D,E) is comprised of interlayered VB and CL layers (Fig. 5A-E). The breccia layers comprise the bottom and top of discrete lava flows, while the coherent lava generally occupies the center of the lava flow where cooling was not as rapid and there was less interaction with the substrate and/or cooling interface (Fig. 5C-G). Jointing is pervasive within the volcanic source rock, but to varying degree depending upon layer composition and corresponding texture. Layers comprised of CL

exhibit the highest fracture density (Fig. 5E,F) and were formed during primary cooling of the lava flow, producing a columnar-style pattern. The CL layers contain numerous intersecting sub-vertical to vertical, to curvilinear joint sets, with spacing rarely exceeding ~1-2 m. The small joint spacing imparts a first-order control on CL boulder size and is reflected in the small size range for pre-CES CL boulders. Layers comprised of VB exhibit a lower fracture density, with joints more widely spaced (and irregular in shape), often 5-10 meters or greater apart (Fig. 5D,E). The wider spacing for joints within VB layers promotes greater rockfall boulder volume (see section 4.4. below).

During the CES, rockfall detachment occurred within approximately 9% (by area) of the volcanic source rock overlying the Rapaki study hillslope (Fig. 5A). The volcanic source rock is comprised of 86% VB and 14% CL (VB:CL ratio=~6:1). 69% of the CES detachment areas occurred within VB and the remaining 31% within CL (Fig. 5A). However, 20% of the identified CL source rock detached during the CES, while only 7% of the identified VB source rock detached during the CES, indicating the CL lithology was more susceptible to detachment.

We were unable to conduct a source rock investigation at Purau with the same spatial resolution as Rapaki because we considered the areal extent of the bedrock source cliffs to be too large at Purau to address in this study and there were safety concerns relating to access and potential for further rockfalls. However, some observations were made for the Purau source rock (Fig. 5D,E) as well as other volcanic coastal cliff outcrops at Sumner (Fig. 5F) and Red Cliffs (Fig. 5G). Field observations indicate that CL layers at Purau are not as prevalent as (and generally thinner than) VB layers, but in some cases may exceed a thickness of 5 meters, which is thicker than CL layers observed at Rapaki (see Fig. 5B,C). At Sumner and Redcliffs, VB and CL layers display roughly equivalent thicknesses (~2-3 m), a condition not apparent at Rapaki or Purau. The variability in layer thickness presumably reflects differences in proximity to source vents and differing conditions during primary cooling of the lava flows.

4.4 Boulder volume

The size and frequency-volume distributions for pre-CES and CES rockfall boulders (for volume ≥ 1.0 m^3) at Rapaki and Purau display similarity (Fig. 8A,C) and can be modeled using power law functions (Fig. 8B,D), with the number of rockfall boulders decreasing significantly

414 as volume increases. Overall, statistical coherence is observed at the 25th, median, and 75th
415 percentile boulder sizes; however, pre-CES rockfalls are consistently higher for each of the
416 size categories at the two study locations (Table 1). Rapaki displays the highest pre-CES to
417 CES variance for 25th, median, and 75th percentiles, while Purau records the biggest pre-CES
418 to CES variance for the average, 95th percentile, and maximum boulder volumes (Table 1, Figs.
419 8A,C). An inter-site comparison of rockfall volumes indicates that pre-CES rockfalls at Rapaki
420 are greater for the 25th, median, and 75th percentile sizes (Table 1) while Purau exhibits larger
421 sizes for the 95th percentile, maximum, and mean boulder categories (Table 1). For CES
422 boulders, the 25th, median, 75th, and 95th percentile Rapaki CES boulders are slightly larger
423 compared with Purau CES boulders, while the maximum and mean boulder size categories are
424 higher at Purau (Table 1). Although differences are evident, the overall size distributions are
425 comparable (Table 1).
426
427 The volume for pre-CES and CES VB boulders is significantly larger than the corresponding
428 CL boulders at Rapaki (Fig. 8E, Table 2) and Purau (Fig 8F, Table 2). At Rapaki, pre-CES VB
429 boulders display higher volumes (compared with CES VB boulders) in each of the size
430 categories, particularly for median and maximum boulder sizes (Table 2). Pre-CES CL
431 boulders display consistently higher values for each of the size categories with the exception
432 of the 75th percentile (Fig. 8E, Table 2). At Purau, CES VB and CL boulders exhibit a smaller
433 distribution of boulder sizes compared with their pre-CES equivalents (see Fig. 8F). Pre-CES
434 VB and CL boulders are higher in each of the size categories (Table 2, Fig. 8F), with the
435 exception of the median boulder size, where the CES CL median boulder volume is slightly
436 more than the pre-CES CL value (Table 2). It is notable that the highest percent (%) variance
437 in boulder volume between pre-CES and CES boulders is recorded for the Purau VB boulders
438 (Table 2); the only exception is for maximum boulder size, where the percent (%) difference
439 between Purau CL pre-CES and CES boulders is even greater (Table 2).
440
441 The volume and frequency ratios for pre-CES and CES rockfall boulders are plotted in Figure
442 9A. The pre-CES to CES boulder volume ratios at Rapaki and Purau range from ~8-12 and ~7-
443 37, respectively (Table 3A, Fig. 9A). The corresponding frequency ratios are consistently
444 lower, ranging from ~6-8.5 and ~3.5-27.5 (Table 3A, Fig. 9A). Overall, the boulder volume
445 and frequency ratios are greater at Rapaki, with the exception of the CL lithology (Tables 3B,
446 3A, and Fig. 9A).
447

448 The calculation of VB and CL boulder percentages at Rapaki for pre-CES and CES rockfalls
449 indicates that VB boulders comprise ≥ 98% by volume and ≥ 94% by frequency (n) for all
450 Rapaki conditions, while at Purau the corresponding percentages are ≥ 90% (volume) and ≥
451 64% (frequency), respectively (Table 3B). All of the lowest VB percentages exist at the Purau
452 study location (see Table 3B, individual domain data).
453
454 **4.5 Boulder runout distance**
455
456 The frequency-runout distance distribution for pre-CES boulders at Rapaki can be
457 characterized by power and exponential laws (Fig. 9B), with the number of rockfall boulders
458 with long runout distances decreasing dramatically with increasing distance from the volcanic
459 source rock. The exponential regression is best fit to the entire data set (including extrapolated
460 boulders within 100 m of source rock), while the power law displays the strongest fit for the
461 mapped rockfall boulders (Fig. 9B). CES rockfalls display a poor exponential fit and do not
462 indicate a similar inverse relationship between boulder frequency and runout distance (Fig.
463 9B). The frequency-runout distribution for CES rockfalls indicates that the number of boulders
464 remains more or less consistent regardless of distance from the source rock. Using the shadow
465 angle method, we plot travel distance on the talus slope (Lt) versus height on the talus slope
466 (Ht) with a fitted polynomial regression line (Fig. 9C). The correlation coefficient is 0.9699 for
467 CES rockfalls and 0.9717 for pre-CES rockfalls (Fig. 9C). The minimum shadow angle for
468 pre-CES is 25°, while the minimum shadow angle (for the furthest traveled CES rockfall
469 boulders) is 23°. At Rapaki, the maximum runout distance for pre-CES and CES VB boulders
470 exceeds the furthest travel distances for pre-CES and CES CL boulders, respectively (Table 4).
471 The CES VB boulders exceed pre-CES VB runout by ~165 meters and CES CL boulders
472 exceed CL pre-CES runout by ~138 meters (Fig. 2A,B; Table 4).
473
474 At Purau, Lt versus Ht is plotted for four (4) separate geomorphic domains (PD1-PD4) to
475 evaluate the distribution of pre-CES and CES boulder runout distances (Fig. 9D; see Fig. 3 for
476 domain locations). The pre-CES and CES rockfalls for the individual domain data sets are
477 characterized by a variety of regression functions with high correlation coefficients (Fig. 9D;
478 Supplementary Data, S24). CES rockfalls in PD1 and PD4 have significantly further maximum
479 runout distances than their pre-CES counterparts, while the inverse is evident in PD2 and PD3.
480 [We note that only two CES boulders were observed in PD2.] The minimum shadow angle for

pre-CES rockfalls at Purau is 25°, while the corresponding minimum CES rockfall shadow angle is 18°. At Purau, the longest recorded runout distances occur for pre-CES CL and VB boulders and CES VB rockfall boulders within PD3 (Table 4).

At Rapaki, no relationship has been obtained plotting individual boulder volumes and the tangent of the shadow angle (Fig. 9E). A wide range of boulder sizes are evident for the full spectrum of pre-CES and CES rockfall runout distances by means of the shadow angle. The same is largely true at Purau, where correlations for the individual domains (PD1-PD4) are poor and the data has a high degree of scatter (i.e. low correlation coefficients); although the data does show a slight negative relationship between block volume and *Ht/Lt* ratio value (that is, a slight increase in runout distance as boulder size increases) (Fig. 9F).

4.6 RAMMS rockfall modelling

4.6.1 RAMMS_1

Final emplacement locations (Q 95%) are generated for simulated rockfalls released from the seven (7) field-identified CES detachment zones at Purau (labeled CES-1 through CES-7) (Fig. 10A). Observed CES boulder locations are depicted as red circles. RAMMS_1 (bare-earth CES model scenario) is successful in replicating the overall spatial pattern for detached and distributed CES rockfalls at Purau for locations CES-3, -4, -5, -6, and -7. Below the CES-7 source rock, RAMMS maximum runout distances (~370 m) are well matched to the maximum travel distance for mapped CES rockfalls (~357 m). Maximum runout distances for the RAMMS boulders are overestimated at CES-1 and CES-2 (Fig. 10A). We note that only 2 boulders were released at CES-1 during the CES and were deposited within ~12 meters of the source rock. RAMMS_1 effectively captures the lateral dispersion for the mapped CES boulders at CES-2, CES-3, and CES-4, but overestimates this effect within the CES-5 and CES-6 valleys, and slightly underestimates the lateral dispersion of CES rockfalls beneath CES-7.

4.6.2 RAMMS_2

The RAMMS_2 model scenario (forested hillslope) is moderately successful (slight overprediction) in replicating the overall spatial distribution and maximum runout distances for the majority of mapped pre-CES rockfalls at Purau (Fig. 10B). The exception is area CES-

7, where RAMMS predicts deposition of pre-CES boulders significantly farther (~325 m) from the source rock than is evident in the field (~80 m). Elsewhere, the greatest variance in maximum runout distance between RAMMS_2 and the mapped pre-CES boulders is ~75-100 m (see Fig. 10B). An increase in forest density to 10,000 kg/s, spread uniformly across the study site, produces the best fit to the pre-CES boulder spatial distributions (in particular, maximum runout distance) (see Figure 10B, white dashed line). RAMMS_2 successfully models the lateral dispersion for the mapped pre-CES boulders (with the exception of area CES-7) (Fig. 10B). The RAMMS_2 model scenarios identify pre-CES rockfall boulders that have likely experienced post-emplacement mobility (see Fig. 10B). Note the collection of pre-CES boulders within the central drainage canyon that exceed the limit of simulated RAMMS boulders (Fig. 10B). Field observations confirm that boulder depositional patterns beyond the limits of the final resting locations for RAMMS simulated rockfall boulders are consistent with deposition by debris flow and other transport/deposition processes. This is further highlighted by the numerous and large pre-CES rafted boulders (maximum volume=20 m^3) identified near the Purau coastline (see Fig. 3). Finally, we observe no mapped pre-CES boulders outside of the valleys that exceed the RAMMS_2 simulated maximum runout distances.

4.6.3 RAMMS_3

RAMMS_3 models the potential future rockfall hazard at Purau and assumes a bare-earth (deforested) hillslope and dry soil moisture conditions to insure a worst-case (conservative) outcome (Fig. 10C). As expected, RAMMS_3 rockfalls obtain higher kinetic energy, velocity, and jump heights than RAMMS_2 boulders (see Supplementary Data, S18, S19), and as a result, runout farther than the RAMMS_2 boulders (Fig. 10B). On average, maximum runout distance for RAMMS_3 boulders is ~450-500 m, representing an increase of ~100-150 m compared with RAMMS_2 boulders, a difference consistent with results from RAMMS numerical modeling at Rapaki (see Borella et al., 2016a). With the exception of area CES-7, RAMMS_3 maximum runout distances are well in exceedance of the mapped locations for the CES rockfall boulders (Figs. 10A,C).

4.7 Strong ground motion data

High frequency data show complex velocity and displacement paths for any given site. The variations across the sites are significant, as reported previously (Van Houtte et al., 2012;

549 Bradley, 2016). At the same site (LPCC, Fig. 7A,B), particle velocity and motion hodograms
550 show different polarization characteristics for different earthquakes. Peak velocities and
551 displacements recorded at LPCC site are higher for the Mw 6.2 than the smaller event Mw 6.0
552 (Fig 7A, B). The observed inter-site and inter-event variations in polarization of peak velocities
553 and displacements can be attributed to source radiation pattern (Lee, 2017) and complex wave
554 propagation effects such as scattering. For instance, simulating high frequency (> 1 Hz) 3-D
555 wavefields, Takemura et al. (2015) showed that near-station irregular topography amplifies
556 scattering of seismic wavefield, producing long coda and distortions to P wave polarizations.
557 This is not surprising given that Fresnel volume – the region to which a transmitting seismic
558 wave is sensitive – is inversely related to wave frequency (Spetzler and Snieder, 2004), due to
559 which near-station geological conditions modify wave characteristics at high frequencies. The
560 control of near-station geology over polarization and amplification characteristics at high
561 frequencies (Bouchon and Barker, 1996) reduces our ability to extrapolate these characteristics
562 to distant sites.
563
564 **5 Discussion**
565
566 **5.1 Rockfall spatial distributions and frequencies**
567
568 At Rapaki, significant differences in spatial distribution between the pre-CES and CES boulder
569 populations are observed (Fig. 2 and Table 4). The increased distance for the CES rockfall
570 boulders is interpreted as an effect of anthropogenic deforestation on the hosting hillslope,
571 which enabled CES boulders to travel further than their pre-CES counterparts due to reduced
572 resistance from vegetation (Borella et al., 2016a). The increase in CES runout distance
573 (~165±15 m) and corresponding reduction in minimum shadow angle resulted in significant
574 impact and damage to homes and infrastructure in the Rapaki village, highlighting the
575 importance of considering the effects that modifications to hillslopes may have on rockfall
576 hazard. At Rapaki, pre-CES VB boulders are present in significantly greater number and have
577 further average and maximum runout distances than the pre-CES CL boulder lithologies (Fig.
578 2A, Table 4). A similar relationship is evident between the CES VB and CL boulders, where
579 CES boulders with the furthest runout distances are exclusively comprised of volcanic breccia
580 (Fig. 2B). It is possible that the reduced runout distances for pre-CES and CES CL boulders is
581 a statistical counting bias (i.e. low number of CL boulders for volume ≥1.0 m^3), but a more

plausible explanation is that the reduced runout distance for CL boulder lithologies is a result of CL boulder shapes being dominated by elongate and flat morphologies (Fig. 4G-K), which would have more difficulty traveling downslope.

At Purau, discerning the differences in spatial distribution between pre-CES and CES rockfalls is more difficult, primarily due to the topographic forcing of rockfalls into nearby drainage valleys and post-emplacement mobilization (Fig. 3). Location CES-7 (furthest southern rockfalls) does show a similar pre-CES:CES spatial scenario to Rapaki, with CES boulders traveling significantly further than their pre-CES equivalents (see Fig. 5); a discrepancy which could also be attributed to intervening deforestation on the hillslope. However, elsewhere at the Purau field site inverse spatial scenarios are evident, with pre-CES boulders deposited further from the source rock than their CES counterparts (see Fig. 2A, Table 4). This is primarily observed within drainage valleys where field observations suggest pre-CES boulders have been remobilized (debris flows, floods) and carried further from the source rock following their initial emplacement.

The CES rockfall boulders at both sites represent a subset of the larger pre-CES rockfall database, suggesting the preservation of multiple pre-CES rockfall events. The ratio for the number of pre-CES to CES rockfall boulders is higher at Rapaki (~8.5:1) than Purau (~5:1) (Table 3, Figs. 2, 3). One cause of the observed difference may be the higher number of CL boulders with size ≥1.0 m^3 at the Purau study site (Fig. 8E,F). At Rapaki, most of the detachment within the CL source rock generated boulder volumes below the 1.0 m^3 threshold. As a result, the ratio of pre-CES VB:CL boulders is significantly higher at Rapaki (~22:1) (Table 3B, Fig. 2A) than Purau (~2:1) (Table 3B, Fig. 3B). This contrasts with the ratio of CES VB:CL boulders at Rapaki (~15:1) (Table 3B, Fig. 2B) which shows near equivalence to Purau (~14:1) (Fig. 3C). The CES VB:CL ratio at Purau is more consistent with our field observations where VB predominates in the source rock. Overall, the results indicate there is a high degree of variability for lithology and discontinuity spacing (e.g. joints) within the source rock and suggests the cumulative ratio of VB:CL boulders can be significantly different from that generated locally during a single rockfall event.

5.2 Boulder morphology and other characteristics

615 The shapes for the VB (Fig. 4A-E) and CL (Fig. 4G-K) boulders are primarily controlled by
616 pre-existing discontinuities (primarily joints) in the source rock. We modeled the influence of
617 boulder shape on spatial distribution for the VB and CL lithologies assuming detachment from
618 the CES-7 site (under bare-earth conditions) using RAMMS (Fig. 11). To eliminate the effect
619 of boulder size, a volume of 1.0 m^3 was assumed for all rockfall boulders. The VB boulders
620 were assigned a range of equant boulder shapes, while CL boulders were assigned only
621 elongate and flat boulder morphologies. The model results highlight the differences in boulder
622 spatial distribution resulting from differences in boulder shape, with equant (VB) boulder
623 lithologies displaying a significantly higher relative percentage of longer runout distances (Fig.
624 11A) compared with the elongate/flat (CL) boulder morphologies (Fig. 11B). We recognize
625 that the modeling represents an ideal scenario (i.e. other transition morphologies do exist for
626 the VB and CL boulders) and was conducted primarily to provide a sense for the expected
627 spatial patterns assuming the distinct VB and CL boulder shapes. Further work is required to
628 verify coherence between field observations and model results.
629
630 **5.3 Source rock characteristics**
631
632 The VB and CL percentages in the Rapaki source rock (86% VB and 14% CL) are lower than
633 the corresponding VB and CL percentages determined from rockfall frequency and volume for
634 the pre-CES (96% VB and 4% CL) and CES (94% VB and 6% CL) rockfalls. We attribute the
635 percent differences between source rock and rockfalls to the influence of the larger VB boulder
636 sizes and the lower number of CL rockfalls meeting the ≥ 1.0 m^3 size threshold. These two
637 factors also explain detachment during the CES, where 69% of the detachment areas occurred
638 within VB and the remaining 31% within CL (Fig. 5A-C), yielding a lower VB:CL ratio of
639 ~2:1 compared with the corresponding boulder volume and frequency ratios (~15:1 and ~52:1,
640 respectively) (Table 3B).
641
642 **5.4 Boulder volume**
643
644 The size and frequency-volume distributions for pre-CES and CES rockfalls at the two study
645 sites can be modeled using a power law (Figs. 8A-D); a relationship that is well-established
646 (e.g. Dussauge-Peisser et al., 2002; Guzzetti et al., 2002) for rockfalls globally and has also
647 been successfully applied for CES rockfalls in Banks Peninsula (Massey et al., 2014). The net

increase in volume distribution for pre-CES boulders could represent a statistical effect and reflect the inclusion of more boulders into the rockfall data set through time (which would increase the likelihood of more large boulders) and/or could reflect higher shaking intensities and/or source rock vulnerability during pre-CES events. Variations in CES vs. pre-CES boulder volumetric distributions for the same lithologies could reflect structural and/or more subtle lithologic variability within the source cliffs from which boulders were derived, and/or post-detachment weathering during boulder transport or *in situ*. The significantly higher volumes for VB boulders (pre-CES and CES) at both study sites reflects the predominance of VB within the source rock and wider joint spacing within the thicker VB layers.

5.5 Boulder runout distance

The exponential law fit for pre-CES boulders (Fig. 9B, short dashed blue line) highlights the importance of slope and initial impact velocity at the cliff base, which causes more boulders to be deposited at greater distances and creates a deviation from the power law fit (Fig. 9B, solid blue line). The exponential fit for CES rockfall boulders is poor and indicates there is no discernable correlation between CES boulder frequency and runout distance (Fig. 9B, solid red line). Despite the low number of CES boulders (n=48), it is interesting that the CES runout distribution shows such a noticeable deviation from the pre-CES data set and could reflect the influence of deforestation on runout distance. This would imply that the incremental input of CES and future rockfalls at Rapaki (emplaced during bare-earth conditions) will modify the overall trend for the cumulative rockfall data set.

At Rapaki, the shadow-angle *Ht/Lt* relationship is fit best using a polynomial regression (Fig. 9C). The trend indicates a positive correlation between talus slope height (Ht) and travel distance on the talus slope (Lt), with a reduction in the rate of increase as rockfall runout (Lt) increases. At Purau, CES and pre-CES rockfalls (within individual geomorphic domains) are modeled using a variety of data functions (e.g. linear, log, polynomial), suggesting intra-site geomorphic and geologic factors affecting rockfall hazard are spatially variable **(**Fig. 9D). We note that Copons (2009) reports linear regression lines for historical rockfalls in the Central Pyrenees using the shadow-angle method, and locally, Massey et al. (2014) also show linear regression fits using the shadow-angle method for CES rockfalls in the Port Hills of southern Christchurch. Our data indicates that non-linear regression functions (for the shadow-angle method) are more successful in capturing the Ht/Lt relationship as distance from the source

682 rock increases. At both sites, a wide range of boulder sizes exist for the full spectrum of pre-
683 CES and CES *Ht/Lt* ratios, suggesting that boulder size is not a primary driver for runout
684 distance at the study sites; although it is possible that smaller boulders (e.g. ~1-2 m^3) exhibiting
685 long runout distances (i.e. low *Ht/Lt* ratios) may represent smaller rock fragments detached
686 from larger boulders during transport and eventual emplacement on the hillslopes and within
687 valleys.
688
689 **5.6 RAMMS rockfall modelling**
690
691 **5.6.1 RAMMS_1**
692
693 A primary challenge in replicating the distribution of CES rockfalls was determining an
694 appropriate set of terrain parameters for the drainage valleys (see Appendix 1, Table A1). To
695 match the RAMMS boulders with the field-mapped CES rockfalls (Fig. 10A) it was necessary
696 to create separate valley terrain polygons and modify the terrain parameters to reflect the high
697 degree of impedance and/or dampening (Vick et al., 2019) in the drainage gullies (see
698 Appendix 2, Table A1). Our field observations confirm the presence of abundant pre-existing
699 boulders within drainage valleys (Fig. 12A-F) and many instances where CES boulders were
700 stopped by pre-CES rockfalls (see Fig. 12A-C). The effect of pre-CES rockfall debris on
701 boulder transport and final resting location needs to be further investigated in order to
702 effectively model impediments within drainage valleys. Further, a more refined understanding
703 of the influence that substrate soil moisture content has on rockfall runout is required (Vick et
704 al., 2019). We note that the DEM used for our study has a resolution of 4 m and may not
705 adequately simulate the smaller scale surface roughness (e.g. clustering of boulders below this
706 size threshold) observed during our field studies (Fig. 12A-G).
707
708 **5.6.2 RAMMS_2**
709
710 The best RAMMS_2 model fit occurs when the forest density is increased (to 10,000 kg/s) and
711 applied uniformly across the Purau hillslopes (see Figure 10B, white dashed line). This
712 represents an increase compared with the forest density used at Rapaki (i.e. 3000 kg/s for
713 moderate vegetation [interfluves], 6000 kg/s for dense vegetation [valleys] (see Borella et al.,
714 2016a) and implies that vegetation may have been denser on the northwest-facing Purau
715 hillslopes compared with the south/southeast facing Rapaki hillslope.

716
717 We note the difference between maximum runout distance for RAMMS and empirical pre-
718 CES boulders at the CES-7 site (Fig. 10B). Several possible explanations exist including: (1)
719 pre-CES boulders were in fact deposited further from the source rock and were subsequently
720 buried by loess and hillslope colluvium; (2) RAMMS underestimates the effect of hillslope
721 vegetation at Purau during prehistoric times; (3) during pre-CES times less of the source rock
722 was exposed (due to burial) and therefore the volcanic rock was less susceptible to detachment
723 during shaking; and/or (4) during pre-CES shaking events the direction of strong ground
724 motion was not favorable to rockfall detachment. Scenario 1 is possible but would need to be
725 confirmed through subsurface trenching or ground penetrating radar (GPR) methods. Tunnel
726 gulley erosion has exposed sections of the subsurface on the CES-7 hillslope and no buried
727 boulders are evident. Scenario 2 is probable based on our observations of forested hillslopes
728 elsewhere in the Port Hills and greater Banks Peninsula area. It is common for dense native
729 vegetation to grow up to, and in some cases, onto portions of the volcanic source rock. In these
730 cases, a high volume of detached rockfalls are stopped adjacent to the source rock and never
731 generate the required momentum to runout an appreciable distance. Scenario 3 is also a
732 possibility and requires that the CES-7 source rock was partially buried during emplacement
733 of the pre-CES rockfalls. The last phase of hillslope aggradation would have occurred during
734 the last glacial maximum (~18-24 ka) and possibly up to ~12-13 ka (see Borella et al., 2016b).
735 We assume the Purau hillslopes have been net erosional (i.e. downwasting) since the early
736 Holocene; a condition that would have been significantly accelerated after deforestation in the
737 Purau area. Option 4 is a final possibility but would require that the ~north facing PD1 source
738 rock is oriented in such a way that strong ground motions from multiple prehistoric shaking
739 events were unable to create rockfall detachment to the degree evident in the CES (see section
740 5.7 for more discussion on strong ground motions).
741
742 RAMMS 2 model scenarios effectively identify pre-CES rockfall boulders that have likely
743 experience post-emplacement mobility (Fig. 10B). This is shown by the collection of pre-CES
744 boulders within the central drainage canyon that exceed the limit of simulated RAMMS
745 boulders (Fig. 10B), indicating a transport mechanism other than rockfall. This result has
746 implications for rockfall hazard studies because boulder locations not reflective of cliff
747 detachment and subsequent downslope displacement by bouncing, sliding, and rolling (that is,
748 rockfall) should be excluded from any data set before assessing the potential rockfall hazard
749 and associated risk. Furthermore, paleoseismic studies attempting to determine the timing and

recurrence interval of prehistoric rockfall events should avoid using boulders with complex post-emplacement mobility histories.

The absence of any pre-CES boulders exceeding the RAMMS_2 maximum runout distance (with the exception of rockfalls within valleys) (Fig. 10B) implies that the mapped pre-existing boulders were deposited prior to deforestation of the Purau hillslopes and are prehistoric (i.e. deposited prior to European arrival) in age. This result is consistent with prehistoric boulder ages determined at the Rapaki study site where the youngest emplacement ages for pre-CES boulders are ~2-6 ka (Mackey and Quigley, 2014; Borella et al., 2016b).

5.6.3 RAMMS_3

RAMMS_3 highlights the increased spatial extent (including maximum runout distance) of rockfalls that could result from more widespread detachment within the Purau source rock, particularly for detachment sites overlying hillslopes where boulder trajectories are not as strongly influenced (i.e. captured) by nearby valleys. Although we caution against using RAMMS_3 as a rockfall hazard map, the model results do provide a first-order indicator of low-lying areas that are most susceptible to future rockfall hazard and suggest that development at the S1 and S2 sites could be adversely impacted by future rockfall events (Fig. 10C). Assuming terrain characteristics remain similar, Sites 3, 4, and 5 are unlikely to be impacted by rockfall boulders in the future, although additional mapping and related structural studies of the volcanic source rock is required to determine the most vulnerable rockfall source areas.

5.7 Interpretations of strong ground motion data

Preceding studies provide some insight into possible strong ground motion characteristics at Rapaki and Purau during the Mw 6.0 and 6.2 earthquakes. Kaiser et al.'s (2014) seismic array analysis of weak ground motion provides information regarding frequency-dependent amplification at Kinsey Terrace, Redcliffs, and Mt. Pleasant (henceforth Ksites), all of which are north-facing slopes in the Port Hills. They found that both morphological features as well as properties of the wave propagation media control frequency-dependent amplification. Significant ground motion amplification was observed at 1 – 3 Hz frequency range on top of narrow, steep-sided ridges. At these low frequencies (f), seismic wavelengths (λ) are

783 comparable to ridge width of Ksites. Therefore, seismic waves in the 1 – 3 Hz frequency band
784 appear to excite natural resonance (or natural frequency; f_n), optimizing ground motion.
785
786 It is interesting to evaluate the implications of Kaiser et al.'s (2014) low frequency observations
787 to Rapaki and Purau rockfall sites. Both these sites are located at higher elevations than Ksites.
788 Thus, their ridge width (~400 – 500 m) is somewhat less than that at Ksites (~ 600 – 1000 m).
789 Using this information, we estimate f_n to be < 5 Hz (see Supp. Info.).
790
791 Whether ground motion with f_n was excited at these sites depends on the amount of energy
792 carried by seismic waves in that frequency band. This information is contained in the spectra
793 of velocity seismograms – a proxy for kinetic energy distribution over frequency. We selected
794 D13C station for this preliminary analysis because the distance between this station and the
795 Rapaki site is only about 2 km. They are also at similar elevations with ridge morphologies
796 resembling each other. Rapid variations in geological conditions are unlikely over such short
797 length-scales, which allows us to extrapolate both high and low frequency wave characteristics
798 observed at D13C station to Rapaki with less uncertainty than the other stations. The nearest
799 station to Purau is LPCC (~ 5 km). The two sites are vastly different as LPCC is located at the
800 toe of a steep cliff in the Lyttelton Port, whereas Purau sites are high elevation ridges. Thus,
801 ground motion recorded at LPCC is not a reliable proxy for ground motion characteristics at
802 Purau. The next nearest station D15C is ~ 7 km from Purau and it suffers from morphological
803 dissimilarities (variations in ridgeline orientation and morphology) that make extrapolating
804 ground motion between the sites highly unreliable. Although the D13C station is located ~10
805 km from Purau, the similarity of morphological features including elevation makes D13C a
806 desirable station to understand ground motion at Purau.
807
808 We computed velocity spectra of east and north components of the station D13C (Fig. 13) to
809 qualitatively assess seismic energy transmission through our rockfall sites. We find that the
810 transition from the flat spectrum to a rapid fall off occurs at ~3 – 4 Hz. This means that the 13
811 June 2011 Mw 6 earthquake carried most of its energy at frequencies less than ~3 – 4 Hz.
812 Together with our estimates of f_n (< 5 Hz), we can thus infer that the passage of seismic waves
813 excited natural resonance at Rapaki and Purau sites. The combined effects of natural resonance
814 and wave focusing towards the ridge crest (Hartzell et al., 1994; Bouchon & Barker, 1996) in
815 these hard rock sites have the potential to optimize shaking, promoting rockfalls.
816

817 It is interesting to note, however, that D13C recorded the lowest peak velocities (223 mm/s and
818 178 mm/s) and displacements (38 mm and 74 mm) of the four stations considered here (Fig.
819 7C). Out of these stations, it is also the only station that recorded no acceleration above 0.3g
820 on any component. These features of the wavefield are not surprising because distance from
821 D13 C to epicentre of the Mw 6 earthquake is twice (~9 km) as large as that from the other
822 stations (~4.5 km). For this reason, it is likely that other possible effects (e.g., rockmass
823 weakening by prior CES earthquakes), in addition to strong ground motions from the Mw 6
824 earthquake, were responsible for triggering major rockfalls at the study sites. Unfortunately,
825 D13C was not in operation at the time of these previous larger earthquakes to assess severity
826 of ground motion. Nonetheless, records from stations closest to D13C indicate that those sites
827 have exceeded the 0.3g peak ground acceleration (PGA) threshold important for engineering
828 considerations. For instance, LPCC station located ~6 km from D13C recorded 0.3g and 0.9g
829 PGA following the Mw 7.1 and Mw 6.2 events respectively (Bradley & Cubrinovski, 2011).
830 Moreover, extrapolation of PGA contours of Bradley (2012) suggests that D13C and Rapaki
831 sites experienced PGAs exceeding 0.25g and 0.45g during Mw 7.1 and Mw 6.2 earthquakes
832 respectively. Some of the rockfall sites investigated herein might have had reached a critical
833 failure threshold prior to being triggered by the 13 June 2011 Mw 6 earthquake.
834
835 Particle velocity and motion hodograms (Fig. 7A-E) also carry directional information of
836 particle behavior in addition to intensity. Past studies show that seismic wave polarizations are
837 amplified in directions perpendicular to fracture surfaces, weakening the coherence between
838 outer blocks of rock with bedrock during the passage of a seismic wave (Kleinbrod et al., 2017;
839 Burjánek et al., 2018). If blocks of rock are primed for failure by previous events, this effect
840 can produce rockfalls in earthquakes as small as local magnitude 4.0 (Keefer, 1984). The
841 velocity hodogram of D13C exhibits a strong ENE-WSW component. Note that this direction
842 makes roughly ~30º to ~60º angle with rock faces at PD2, PD3, PD4, and RAP sites (Fig. 7C).
843 Thus, it is reasonable to assume that particle velocities in this dominant direction are favorable
844 for triggering rockfalls particularly if the rock faces were primed for failure. The angle between
845 this dominant velocity component and the rock face at PD1 site, however, appears to be less
846 than ~20º and possibly is not as favorable for triggering rockfalls as for other sites. On the other
847 hand, the particle motion hodogram has two dominant directions; WNW and WSW. Depending
848 on the strike of the rock face, either one of these directions can orient particle motion favorably
849 for rockfalls. For instance, site RAP has a rock face strike of 25º, which is sub-parallel to the
850 WSW particle motion direction. However, the WNW particle motion direction makes a steep

angle with the rock face and thus can promote rockfalls. Combining information from particle velocity and motion hodograms, we hypothesize that directional aspects were favorable to rockfall triggering at the Rapaki and Purau sites.

5.8 Pre-existing rockfalls as predictive database

Our study indicates that pre-existing rockfalls provide an accurate range of expected boulder volumes, shapes, and % lithologic variance (i.e. VB vs CL) but their use as a spatial indicator for future rockfalls should be approached with caution because there are a variety of geologic and anthropogenic factors that influence the final resting location for rockfalls. These factors include changes to the rockfall source (i.e. emergence of bedrock sources from beneath sedimentary cover), remobilization of prior rockfalls by surface processes including debris flow transport, collisional impedance with pre-existing boulders, potential natural and human-induced landscape changes (including deforestation), and variations in the location, size, and strong ground motion characteristics of past rockfall-triggering earthquakes. Our study indicates that pre-CES rockfalls underestimated the expected average and maximum runout distances on interfluves, in part, because pre-CES rockfalls were probably emplaced on a forested hillslope. Conversely, the locations for pre-CES boulders in well-established drainage valleys/channels may overestimate the expected runout for future rockfalls because the rockfalls have been remobilized after their initial emplacement.

Prior to the CES, rockfall hazard was not considered a major risk in Banks Peninsula and surrounding areas (Townsend and Rosser, 2012), including the Port Hills of southern Christchurch, where damage was most critical and 5 fatalities occurred (Massey et al., 2014). To date, we are aware of only four studies that have dated pre-CES rockfalls in Banks Peninsula (Mackey and Quigley, 2014; Borella et al., 2016b, Sohbati et al., 2016; Litchfield et al., 2016), and all of these investigations were undertaken after the CES. We assume this was primarily because there were few records of historical rockfall occurrence, and of those described (Lundy, 1995), none hinted at the potential for future widespread cliff collapse and rockfall in the region. However, the geologic record (i.e. prehistoric rockfalls) provides evidence that rockfall events of similar magnitude (or greater) have occurred in the past. In regions devoid of historical or contemporary rockfalls, pre-existing rockfalls represent the only empirical proxy for evaluating local rockfall behavior and provide valuable input for rockfall modeling and risk assessment studies. Existing rockfalls provide important data for predicting rockfall

volumetric, lithologic, and morphologic (i.e. boulder shape) characteristics, but a thorough consideration of landscape evolutionary chronologies (including deforestation) and post-emplacement mobility scenarios is required before pre-existing rockfalls can be confidently used as future spatial indicators.

6 Conclusions

The spatial distributions and physical-geological properties of individual (n=1093) rockfall boulders deposited at two sites in Banks Peninsula prior to the 2010-2011 Canterbury earthquake sequence (CES) are compared to boulders (n=185) deposited during the CES. Pre-CES to CES boulder ratios range between ~5:1 and 8.5:1 respectively, suggesting preservation of multiple pre-CES rockfall events with a flux analogous to or smaller than CES events, and/or pre-CES event(s) of larger flux. Pre-CES and CES boulders at one site (Purau site) have statistically-consistent power-law frequency-volume distributions between 1.0 to >100.0 m^3. At the Rapaki site, CES boulders have smaller and more clustered volumetric distributions that are less well fit by power-laws compared with the pre-CES data, interpreted to reflect variations in rockfall source characteristics through time. Boulders of volcanic breccia (VB) have a larger binned-percentage of large volume boulders and more equant boulder aspects relative to coherent lava (CL) boulder lithologies at both sites, revealing lithologic controls on rockfall physical properties. The maximum runout distances for Rapaki CES VB and CL boulders are greater than that of pre-CES boulders of equivalent lithologies, volumes and morphologies. This is interpreted as an effect of anthropogenic deforestation on the hosting hillslope, which enabled CES boulders to travel further than their pre-CES counterparts due to reduced resistance from vegetation. At Purau, isolated geomorphic domains exhibit this same effect, however in other intra-site locations, pre-CES boulder locations exceed runout distances of CES boulders. This is interpreted to reflect post-depositional mobility of prehistoric boulders via debris flows and other surface processes, reduction of CES boulder runouts in channels due to collisional impedance from pre-CES boulders, and heterogeneity in the CES boulder distributions, which reduced the likelihood of large runout boulders occurring due to smaller volumetric fluxes. The shadow angle method is a reliable predictor for pre-CES and CES rockfall runout at both sites. At Rapaki, the pre-CES and CES rockfall data is best fit using a 2nd order polynomial regression, while at Purau rockfalls require a variety of data fits (e.g. linear, log, polynomial), suggesting intra-site geomorphic and geologic factors affecting rockfall hazard are spatially variable. Bare-earth and forested numerical modeling suggest that

the majority of pre-CES rockfalls were emplaced before deforestation of the Purau hillslopes and enables identification of boulder sub-populations that have likely experienced post-emplacement mobility. The RAMMS_3 model effectively shows the potential spatial extent of rockfalls that could result from more widespread detachment within the Purau source rock and provides a preliminary indicator of low-lying areas most susceptible to future rockfall hazard. More in-depth rockfall hazard analyses (including numerical rockfall modeling) are required at Purau and should consider the implementation of boulder morphologies, terrain parameters, and hillslope vegetation attributes developed in this study. Our research highlights the challenges of using rockfall distributions to characterize future rockfall hazards in the context of geologic and geomorphic variations, including natural and anthropogenically-influenced landscape changes.

Acknowledgements

Financial support for the project came from the New Zealand Earthquake Commission Capability Fund and Port Hills Champion Sue Stubenvoll. J.B. thanks Louise Vick, Sarah Trutner, Peter Borella, Maxwell Borella, David Jacobson, Sarah Bastin, Jonathan Davidson, Peter Almond, Simon Brocklehurst, David Bell, and Jarg Pettinga. Special thanks to Pip and David Barker for allowing land access in Purau and review of the Camp Bay geotechnical property report. We also thank the Rapaki landowners and farmers for land access. The authors declare that they have no conflict of interest.

Author Contribution

J.B. performed the field mapping, RAMMS modeling, and was the primary contributor to the data interpretation and manuscript authorship. M.Q. contributed to study design, data interpretation and manuscript authorship. Z.K. performed field mapping, RAMMS modeling, and contributed to the preparation of the manuscript. K.L. conducted the source rock characterization at Rapaki. J.A. performed the strong ground motion analysis and contributed to the preparation of the manuscript. L.S., H.L., and S.L. performed field mapping of rockfalls at Purau and/or Rapaki. S.H. and D.G. performed field work and contributed to the manuscript preparation.

References

Agliardi, F. and Crosta, G. B.: High resolution three-dimensional numerical modeling of rockfalls, Int. J. Rock Mech. Min. Sci., 40, 455–471, doi:10.1016/S1365-1609(03)00021-2, 2003.

Bartelt, P., Buehler, Y., Christen, M., Deubelbeiss, Y., Graf, C., and McArdell, B. W.: RAMMS - rapid mass movements simulation: A numerical model for rockfall in research practice, User Manual v1.5. Davos, Switzerland, 102 pp., 2013.

Bell, D. H. and Trangmar, B. B.: Regolith materials and erosion processes on the Port Hills, Christchurch, New Zealand, Fifth International Symposium on Landslides, Lausanne: A. A. Balkema, 93-105, 1987.

Borella J., Quigley M., and Vick, L.: Anthropocene rockfalls travel farther than prehistoric predecessors, Sci. Adv., 2, e1600969, 2016a.

Borella, J., Quigley, M., Sohbati, R., Almond, P., Gravley, D.M., and Murray, A.: Chronology and processes of late Quaternary hillslope sedimentation in the eastern South Island, New Zealand, J. Quat. Sci., 31, 691-712, doi: 10.1002/jqs.2905, 2016b.

Bouchon, M. and Barker, J. S.: Seismic response of a hill: The example of Tarzana, California, Seismol. Soc. Am. Bull., 86, 66 – 72, 1996.

Bradley, B. A. and Cubrinovski, M.: Near-source strong ground motions observed in the 22 February 2011 Christchurch earthquake, Seismol. Res. Lett., 82, 853 – 865, https://doi.org/10.1785/gssrl.82.6.853, 2011.

Bradley, B. A.: Ground motions observed in the Darfield and Christchurch earthquakes and the importance of local site response effects, New. Zeal. J. Geol. Geop., 55(3), 279 – 286, https://doi.org/10.1080/00288306.2012.674049, 2012.

Bradley, B. A.: Strong ground motion characteristics observed in the 13 June 2011 Mw 6.0 Christchurch, New Zealand earthquake, Soil. Dyn. Earthq. Eng., 91, 23 – 38, http://dx.doi.org/10.1016/j.soildyn.2016.09.006, 2016.

Burjánek, J., Gischig, V., Moore, J. R. and Fäh, D.: Ambient vibration characterization and monitoring of a rock slope close to collapse, Geophys. J. Int., 212, 297 – 310, https://doi.org/10.1093/gji/ggx424, 2018.

Carey, J. M., Misra, S., Bruce, Z. R., and Barker, P. R.: Canterbury Earthquakes 2010/11 Port Hills Slope Stability: Laboratory Testing Factual Report, GNS Science Consultancy Report 2014/53, GNS Science, Lower Hutt, 88 pp., 2014.

Christensen, N. I., Wilkens, R. H. and Blair, S. C.: Seismic velocities, densities, and elastic constants of volcanic breccia and basalts from deep sea drilling project leg 59, Initial Reports of the Deep Sea Drilling Project, LIX, Washington, pp. 515 – 517, 1980.

Copons, R. and Vilaplana, J. M.: Rockfall susceptibility zoning at a large scale: From geomorphological inventory to preliminary land use planning, Eng. Geol., 102, 142–151, 2008.

Copons, R., Vilaplana, J. M., and Linares, R.: Rockfall travel distance analysis by using empirical models (Sola d'Andorra la Vella, Central Pyrenees), Nat. Hazards Earth Syst. Sci. 9, 2107–2118, 2009.

Dorren, L.: A review of rockfall mechanics and modelling approaches, Prog. Phys. Geog., 27, 69–87, 2003.

Dorren, L., Maier, B., Putters, U. S., and Seijmonsbergen, A. C.: Combining field and modelling techniques to assess rockfall dynamics on a protection forest hillslope in the European Alps, Geomorphology, 57, 151-167, doi:10.1016/S0169-555X(03)00100-4, 2004.

Dussauge-Peisser, C., Helmstetter, A., Grasso, J.-R., Hantz, D., Desvarreux, P., Jeannin, M., and Giraud, A.: Probabilistic approach to rock fall hazard assessment: potential of historical data analysis, Nat. Hazards Earth Syst. Sci., 2, 15–26, http://www.nat-hazards-earth-syst-sci.net/2/15/2002/, 2002.

Eliot Sinclair and Partners Ltd., Unpublished Geotechnical Report prepared for Purau Properties Ltd., Camp Bay Road, Purau, 18 pp., 2011.

Evans, S. G. and Hungr, O.: The assessment of rockfall hazard at the base of talus slopes, Can. Geotech. J., 30, 620–636, 1993.

Guzzetti, F., Malamud, B. D., Turcotte, D. L., and Reichenbach, P.: Power-law correlations of landslide areas in central Italy, Earth Planet. Sci. Lett., 195, 169-183, 2002.

Guzzetti, F., Reichenbach, P., and Wieczorek, G. F.: Rockfall hazard and risk assessment in the Yosemite Valley, California, USA, Nat. Hazards Earth Syst. Sci., 3, 491–503, http://www.nat-hazards-earth-syst-sci.net/3/491/2003/, 2003.

Guzzetti, F., Reichenbach, P., and Ghigi, S.: Rockfall hazard and risk assessment along a transportation corridor in the Nera Valley, Central Italy, Environ. Manage., 34, 191-208, doi:10.1007/s00267-003-0021-6, 2004.

Hampton, S.J. and Cole, J.W.: Lyttelton Volcano, Banks Peninsula, New Zealand: Primary volcanic landforms and eruptive centre identification, Geomorphology, 104, 284-298, doi:10.1016/j.geomorph.2008.09.005, 2009.

Hartzell, S. H., Carver, D. L. and King, K. W.: Initial investigation of site and topographic effects, at Robinwood Ridge, Bull. Seismol. Soc. Am., 84, 1336 – 1349, 1994.

Heron, D., Lukovic, B., Massey, C., Ries, W., and McSaveney, M.: GIS modelling in support of earthquake-induced rockfall and cliff collapse risk assessment in the Port Hills, Christchurch. J. Spat. Sci. 59, 313-332, doi: 10.1080/14498596.2014.913509, 2014.

Kaiser, A. E., Holden, C. and Massey, C. I.: Site amplification, polarity and topographic effects in the Port Hills during the Canterbury earthquake sequence, GNS Science Consultancy Report 2014/121, 33 pp., 2014.

Keefer, D.K.: Landslides caused by earthquakes. Geol. Soc. Am. Bull. 95, 406-421, 1984.

Kleinbrod, U., Burjánek, J., and Fäh, D.: On the seismic response of instable rock slopes based on ambient vibration recordings, Earth Planets Space, 69, 1-9, doi:10.1186/s40623-017-0712-5, 2017.

Lan, H., Martin, C. D., Zhou, C., and Lim, C. H.: Rockfall hazard analysis using LiDAR and spatial modeling, Geomorphology, 118, 213-223, doi:10.1016/j.geomorph.2010.01.002, 2010.

Latham, J-P., Munjiza, A., Garcia, X., Xiang, J., and Guises, R.: Three-dimensional particle shape acquisition and use of shape library for DEM and FEM/DEM simulation, Min. Eng., 21, 797-805, doi:10.1016/j.mineng.2008.05.015, 2008.

Lee, S-J.: Lessons learned from source rupture to strong ground motion simulations: An example from Taiwan, Bull. Seismol. Soc. Am., 107, 2106 – 2116, https://doi.org/10.1785/0120170030, 2017.

Leine, R.I., Schweizer, A., Christen, M., Glover, J., Bartelt, P., and Gerber, W.: Simulation of rockfall trajectories with consideration of rock shape, Multibody Syst. Dyn., 32, 241-271, doi:10.1007/s11044-013-9393-4, 2013.

Lied, K.: Rockfall problems in Norway, in: Rockfall dynamics and protective work effectiveness, Instituto Sperimentale Modelli e Structture (ISMES), Bergamo, Italy, 90, 51–53, 1977.

Litchfield, N. J., Van Dissen, R. J., Massey, C. I.: Pre-Christchurch earthquake sequence rockfalls in the Port Hills, Christchurch: Wakefield Avenue Trench, GNS Science Consultancy Report 2016/25, GNS Science, Lower Hutt, 32 pp., 2016.

Mackey, B.H. and Quigley, M.C.: Strong proximal earthquakes revealed by cosmogenic ^{3}He dating of prehistoric rockfalls, Christchurch, New Zealand, Geology, 42, 975–978, 2014.

Massey, C. I., Gerstenberger, M., McVerry, G., and Litchfield, N.: Canterbury earthquakes 2010/11 Port Hills slope stability: additional assessment of the life-safety risk from rockfalls (boulder rolls). GNS Science Consultancy Report 2012/214, GNS Science, Lower Hutt, pp. 18, 2012a.

Massey, C. I., McSaveney, M. J., Heron, D., and Lukovic, B.: Canterbury earthquakes 2010/11 Port Hills slope stability: pilot study for assessing life-safety risk from rockfalls (boulder rolls). GNS Science Consultancy Report 2011/311, GNS Science, Lower Hutt, pp. 74, 2012b.

Massey, C. I., McSaveney, M. J., Yetton, M. D., Heron, D., Lukovic, B., and Bruce, Z. R. V.: Canterbury earthquakes 2010/11 Port Hills slope stability: pilot study for assessing life-safety

risk from cliff collapse. GNS Science Consultancy Report 2012/57, GNS Science, Lower Hutt, pp. 101, 2012c.

Massey, C. I., McSaveney, M. J., Lukovic, B., Heron, D., Ries, W., Moore, A., and Carey, J.: Canterbury earthquakes 2010/11 Port Hills slope stability: life-safety risk from rockfalls (boulder rolls). GNS Science Consultancy Report 2012/123. GNS Science, Lower Hutt, pp. 34, 2012d.

Massey, C. I., McSaveney, M. J., and Heron, D.: Canterbury earthquakes 2010/11 Port Hills slope stability: life-safety risk from cliff collapse in the Port Hills, GNS Science Consultancy Report 2012/124, GNS Science, Lower Hutt, pp 35., 2012e.

Massey, C. I., Yetton, M. J., Carey, J., Lukovic, B., Litchfield, N., Ries, W., and McVerry, G.: Canterbury earthquakes 2010/11 Port Hills slope stability: stage 1 report on the findings from investigations into areas of significant ground damage (mass movements), GNS Science Consultancy Report 2013/317, GNS Science, Lower Hutt, pp. 37, 2013.

Massey, C. I., McSaveney, M. J., Taig, T., Richards, L., Litchfield, N. J., Rhoades, D. A., McVerry, G. H., Lukovic, B., Heron, D. W., Ries, W., and Van Dissen, R. J.: Determining rockfall risk in Christchurch using rockfalls triggered by the 2010-2011 Canterbury earthquake sequence, Earthquake Spectra, 30, 155-181, DOI: 10.1193/021413EQS026M, 2014.

Massey, C., Della Pasqua, F., Holden, C., Kaiser, A., Richards, L., Wartman, J., McSaveney, M. J., Archibald, G., Yetton, M., and Janku, L.: Rock slope response to strong earthquake shaking, Landslides, 14, 249-268, doi:10.1007/s10346-016-0684-8, 2017.

Muktar, J-A. S.: Engineering geological and geotechnical characterization of selected Port Hills lavas, Master's thesis, Department of Geological Sciences, University of Canterbury, New Zealand, pp. 172, 2014.

Porter, S. C. and Orombelli, G.: Alpine rockfall hazards: Recognition and dating of rockfall deposits in the western Italian Alps lead to an understanding of the potential hazards of giant rockfalls in mountainous regions, Am. Sci., 69, 67-75, https://www.jstor.org/stable/27850249, 1981.

Quigley M. C., Hughes, M. W., Bradley, B. A., van Ballegooy, S., Reid, C., Morgenroth, J., Horton, T., Duffy, B., and Pettinga, J. R.: The 2010-2011 Canterbury Earthquake Sequence: Environmental effects, seismic triggering thresholds and geological legacy, Tectonophysics, 672-673, 228-274, 2016.

Sewell, R.J.: Late Miocene volcanic stratigraphy of central Banks Peninsula, Canterbury, New Zealand, New Zeal. J. Geol. Geop., 31, 41-64, doi:10.1080/00288306.1988.10417809, 1988.

Sohbati, R., Borella, J., Murray, A., Quigley, M., Buylaert, J.: Optical dating of loessic hillslope sediments constrains timing of prehistoric rockfalls, Christchurch, New Zealand. Journal of Quaternary Science, 31, 678-690, doi: 10.1002/jqs.2895, 2016.

Spetzler, J. and Snieder, R.: The Fresnel volume and transmitted waves, Geophysics, 69, 653 – 663, https://doi.org/10.1190/1.1759451, 2004.

Stock, G. M., Luco, N., Collins, B. D., Harp, E. L., Reichenbach, P., Frankel, K. L.: Quantitative rock-fall hazard and risk assessment for Yosemite Valley, Yosemite National Park, California: U.S. Geological Survey Scientific Investigations Report 2014-5129, 52 pp., 2014.

Takemura, S., Furumura, T. and Maeda, T.: Scattering of high-frequency seismic waves caused by irregular surface topography and small-scale velocity inhomogeneity, Geophys. J. Inter., 201, 459–474, https://doi.org/10.1093/gji/ggv038, 2015.

Townsend, D. B., Rosser, B.: Canterbury earthquakes 2010/2011 Port Hills slope stability: Geomorphology mapping for rockfall risk assessment, GNS Science Consultancy Report 2012/15, GNS Science, Lower Hutt, pp. 21, 2012.

Van Houtte, C., Ktenidou, O.-J., Larkin, T., and Kaiser, A.: Reference stations for Christchurch, Bull. New Zeal. Soc. Earthq. Eng., 45, 184 – 195, 2012.

Varnes, D. J.: Slope movement types and processes, in: Landslides: analysis and control, edited by: Schuster, R. L. and Krizek, R. L., Transportation Research Board, National Research Council, Washington, special report 176, 11–33, 1978.

Vick, L.M.: Evaluation of field data and 3D modelling for rockfall hazard assessment, Ph.D. thesis, Department of Geological Sciences, University of Canterbury, New Zealand, pp. 173, 2015.

Vick, L.M., Zimmer, V., White, C., Massey, C., and Davies, T.: Significance of substrate soil moisture content for rockfall hazard assessment, Nat. Hazards Earth Syst. Sci., 19, 1105-1117, 2019.

Wieczorek, G. F.: Catastrophic rockfalls and rockslides in the Sierra Nevada, USA. Geol. Soc. Am. Rev Eng. Geol., 15, 1-26, 2002.

Wieczorek, G. F., Stock, G. M., Reichenbach, P., Snyder, J. B., Borchers, J.W., and Godt, J.W.: Investigation and hazard assessment of the 2003 and 2007 Staircase Falls rock falls, Yosemite National Park, California, USA, Nat. Hazards Earth Syst. Sci., 8, 421–432, http://www.nat-hazards-earth-syst-sci.net/8/421/2008/, 2008.

	Rapaki Pre-CES (n=409)	*Rapaki CES (n=48)*	*Difference*	*Difference*	*Purau Pre-CES (n=684)*	*Purau CES (n=136)*	*Difference*	*Difference*
	(m^3)	(m^3)	(m^3)	(%)	(m^3)	(m^3)	(m^3)	(%)
25th (Q1)	1.60	1.36	0.24	17.65	1.42	1.34	0.08	5.97
Median	2.94	2.21	0.73	33.03	2.20	2.01	0.19	9.45
75th (Q3)	6.59	4.83	1.76	36.44	5.08	4.46	0.62	13.90
95th	20.54	19.76	0.78	3.95	27.06	17.66	9.4	53.23
Maximum	200.56	28.35	172.21	607.44	616.00	79.97	536.03	670.29
Mean	6.81	4.84	1.97	40.70	8.10	5.32	2.78	52.26

Table 1. Volumetric comparison of pre-CES and CES rockfall boulders (for volume ≥1.0 m^3) at Rapaki and Purau study sites.

	Rapaki				***Purau***			
	Pre-CES	CES	Pre-CES	CES	Pre-CES	CES	Pre-CES	CES
	VB (n=391) (m^3)	VB (n=45) (m^3)	CL (n=18) (m^3)	CL (n=3) (m^3)	VB (n=436) (m^3)	VB (n=127) (m^3)	CL (n=248) (m^3)	CL (n=9) (m^3)
25th (Q1)	1.68	1.39	1.22	1.03	1.70	1.36	1.20	1.13
Median	3.1	2.21	1.38	1.06	3.21	2.04	1.56	1.68
75th (Q3)	6.78	5.7	1.54	1.67	7.65	4.87	2.30	2.14
95th	21.28	20.576	3.92	2.16	40.91	17.78	5.26	2.48
Maximum	200.56	28.35	9.99	2.28	616.00	79.97	26.21	2.64
Mean	7.03	5.06	1.96	1.45	11.43	5.58	2.24	1.67
Total volume	2749.07	227.80	35.29	4.34	4938.76	708.34	555.63	15.00
% of total volume	99	98	1	2	89	98	11	2
% of mapped boulders	96	94	4	6	64	93	36	7

Table 2. Comparison of boulder size statistics for Rapaki and Purau VB and CL pre-CES and CES rockfall boulders (volume ≥1.0 m^3).

	# of pre-CES rockfalls : # of CES rockfalls	*pre-CES : CES*	*pre-CES : CES*	*volume of pre-CES rockfalls: volume of CES rockfalls*	*pre-CES : CES*	*pre-CES : CES*
	(n)	ratio	% : %	(m^3)	ratio	% : %
Total (Rapaki + Purau)	1093 : 184	5.94	86 : 14	8323.76 : 955.48	8.71	90 : 10
Rapaki Total	409 : 48	8.52	89 : 11	2784.37 : 232.14	11.99	92 : 8
Rapaki VB	391 : 45	8.69	90 : 10	2749.07 : 227.80	12.07	92 : 8
Rapaki CL	18 : 3	6.00	86 : 14	35.29 : 4.34	8.14	89 : 11
Purau Total	684 : 136	5.03	83 : 17	5539.39 : 723.35	7.66	88 : 12
Purau VB	436 : 127	3.43	77 : 23	4983.76 : 708.34	7.04	88 : 12
Purau CL	248 : 9	27.56	96 : 4	555.63 : 15.00	37.04	97 : 3

Table 3A. Comparison of frequency (n) and volume (m^3) ratios for pre-CES and CES rockfall boulders at the Rapaki and Purau study sites.

	# of VB boulders : # of CL boulders	*VB : CL*	*VB : CL*	*Volume of VB boulders : volume of CL boulders*	*VB:CL*	*VB:CL*
	n : n	ratio	% : %	m^3 : m^3	ratio	% : %
Total (Rap + Purau)	999 : 278	3.59	78 : 22	8668.97 : 610.26	14.21	93 : 7
Rapaki Total (pre-CES + CES)	436 : 21	20.76	95: 5	2976.87 : 39.63	75.11	99 : 1
Rapaki pre-CES	391 : 18	21.72	96 : 4	2749.07 : 35.29	77.9	99 : 1
Rapaki CES	45 : 3	15	94 :6	227.80 : 4.34	52.49	98 : 2
Purau Total (pre-CES + CES)	563 : 257	2.19	69 : 31	5692.1 : 570.63	9.98	91 : 9
Purau pre-CES	436 : 248	1.76	64 : 36	4983.76 : 555.63	8.97	90 : 10
Purau CES	127 : 9	14	93 : 7	708.34 : 15.00	47.22	98 : 2
Purau D1 pre-CES	17 : 0	N/A	100 : 0	137.27 : 0	N/A	100 : 0
Purau D1 CES	30 : 0	N/A	100 : 0	125.86 : 0	N/A	100 : 0
Purau D2 pre-CES	36 : 3	12	92 : 8	230.8 : 3.9	59.18	98 : 2
Purau D2 CES	1 : 1	1	50 : 50	14.78 : 1.08	13.69	93 : 7
Purau D3 pre-CES	54 : 43	1.26	56 : 44	203.79 : 142.62	1.43	59 : 41
Purau D3 CES	38 : 3	12.67	93 : 7	242.63 : 5.91	41.05	98 : 2
Purau D4 pre-CES	8 : 1	8	89 : 11	188.42 : 1.24	151.95	99 : 1
Purau D4 CES	36 : 0	N/A	100 : 0	267.76 : 0	N/A	100 : 0

Table 3B. Comparison of VB/CL frequency (n) and volume (m^3) ratios for pre-CES and CES rockfall boulders at the Rapaki and Purau study sites.

Runout Distance (MLR)	*Average* (m)	*Maximum* (m)
Rapaki		
Pre-CES	184.30	567.51
CES	276.23	702.47
Pre-CES VB	*184.65*	*567.51*
Pre-CES CL	*176.57*	*346.73*
CES VB	*276.91*	*702.47*
CES CL	*266.13*	*432.14*
Purau		
PD1 Pre-CES	29.86	96.96
PD1 CES	119.63	348.4
PD2 Pre-CES	84.01	279.75
PD2 CES	14.11	15.91
PD3 Pre-CES	239.62	462.8
PD3 CES	237.24	413.35
PD4 Pre-CES	109.11	208.85
PD4 CES	181.75	304.56
PD1 Pre-CES VB	29.86	96.96
PD1 CES VB	119.63	348.4
PD1 Pre-CES CL	*N/A*	*N/A*
PD1 CES CL	*N/A*	*N/A*
PD2 Pre-CES VB	*88.73*	*279.75*
PD2 CES VB	*12.3*	*12.3*
PD2 Pre-CES CL	*27.39*	*33.38*
PD2 CES CL	*15.91*	*15.91*
PD3 Pre-CES VB	*248.96*	*434.85*
PD3 CES VB	*243.21*	*413.35*
PD3 Pre-CES CL	*227.89*	*462.8*
PD3 CES CL	*161.68*	*178.53*
PD4 Pre-CES VB	*106.99*	*208.85*
PD4 CES VB	181.75	304.56
PD4 Pre-CES CL	*126.06*	*126.06*
PD4 CES CL	*N/A*	*N/A*

MLR = Map Length Runout
PD1 = Purau Domain 1

Table 4. Average and maximum runout distances for pre-CES and CES rockfall boulders (for volume ≥1.0 m^3) at Rapaki and Purau study sites.

Figure Captions

Fig. 1. **(A)** Google Earth image showing Rapaki and Purau study sites. CES rockfall locations as mapped by GNS Science and the author (at Rapaki and Purau) are shown (red). Epicenter locations for 22 February, 13 June, and 16 April 2011 events are displayed [Modified from Massey et al. (2014)]. Inset map of South Island (New Zealand) shows Banks Peninsula and approximate location for study site (yellow star). **(B)** Anthropogenic deforestation of Banks Peninsula. Removal of native forest occurred rapidly in Banks Peninsula (BP) with arrival of Polynesians (c. AD 1280) then Europeans (c. AD 1830). Before Polynesian (Maori) arrival, extensive native forest was present throughout BP. Prior to European settlement, minor to moderate removal of indigenous forest by Maori occurred, with burning being the primary tool for clearance (yellow). By 1920 Europeans had removed >98% of BP native forest (red). Minor re-establishment of old-growth native forest has occurred (green) but slopes in the Port Hills and greater BP (including Rapaki and Purau) remain largely unvegetated.

Fig. 2. **(A)** Mapped pre-CES volcanic breccia (VB) and coherent lava (CL) boulders with volume ≥1.0 m^3 at Rapaki. The largest boulders with the furthest runout distances are comprised exclusively of volcanic breccia. Ratio of pre-CES VB to CL boulders is ~22:1. **(B)** Mapped CES VB and CL boulders at Rapaki study site. Note the low number of CL rockfall boulders detached during the CES at Rapaki. Ratio of CES VB to CL boulders is 15:1. [a = volcanic source rock; b = dominated by volcanic boulder colluvium and volcanic loess colluvium; c = loess-colluvium underlain by in-situ loess and volcanic rock; d = alluvial sediments overlying loess and bedrock]

Fig. 3. **(A)** Mapped pre-CES and CES rockfalls with volume ≥1.0 m^3 at Purau study site. Ratio of pre-CES to CES boulders is ~5:1. [a = volcanic source rock; b = dominated by volcanic boulder colluvium and volcanic loess colluvium; c = loess-colluvium underlain by in-situ loess and volcanic rock; d = alluvial sediments overlying loess and bedrock] **(B)** Mapped pre-CES VB and CL boulders at Purau. Ratio of pre-CES VB to CL boulders is ~2:1. **(C)** Mapped CES VB and CL boulders at Purau study site. Note the low number of CL rockfall boulders detached during the CES at Purau. Ratio of CES VB to CL boulders is ~14:1. PD1-PD4 represent Purau rockfall domains.

Fig. 4. Pre-CES and CES VB boulders at Rapaki and Purau study sites. **(A)** Pre-CES boulder in footslope position with smaller CES boulder at right bottom. **(B)** Exploratory trenching exposes the colluvial sediment wedge at the backside (upslope) of the boulder. **(C)** Pre-CES boulder at Purau study site. Erosion of the surrounding hillslope sediments has exposed the boulder base and underlying loessic sediment. **(D)** Advanced surface roughness and abundant lichen growth on pre-CES boulder surface. **(E)** CES boulder (~28 m^3) detached from Mount Rapaki and emplaced in the Rapaki village during the 22 February 2011 earthquake (photo courtesy of D.J.A. Barrell, GNS Science). **(F)** CES boulder showing 2011 detachment surface [1] and adjacent non-detached surface [2] with higher degree of surface roughness. **(G-K)** Representative CL boulders at Rapaki and Purau sites exhibit typical elongate and flat morphologies.

Fig. 5. **(A)** Volcanic source rock at Rapaki study site. Sixty (60) individual detachment zones were created during the CES (yellow) and represent ~9% of the total source rock area. The source rock is comprised of ~86% VB and ~14% CL. ~69% and ~31% of the detachments occurred within the VB and CL lithologies, respectively. **(B)** Photo showing

several irregularly shaped CES detachment zones near the top of Mt. Rapaki. **(C)** Photo showing freshly exposed VB and CL layering within the Rapaki source rock. **(D)** Portion of volcanic source rock at Purau showing VB and CL layering. A single CES detachment site is shown at the top of the source rock. Seven (7) individual CES detachment sites were identified at the Purau study site. **(E)** CL and VB layers at the Purau study site. Note the thickness of the CL layer (~5-7 meters) and lack of any CES detachment sites despite the high degree of fracturing and overhanging condition. **(F)** VB and CL layering in Sumner (Christchurch) cliff exposure adjacent to Main Road. Extensive cliff collapse during the CES has revealed multiple lava flows and the distinctive textural differences between the VB and CL lithologies. Note the high density of vertical to subvertical fractures within the CL layers. **(G)** Exposed lava layers adjacent to Main Road in Redcliffs (Christchurch). Note the single-family living residence at top of photo.

Fig. 6. Relative locations of stations LPCC, D13C, D15C, and GODS (yellow squares). Also shown are epicentres of 2011-02-22 Mw 6.2 and 2011-06-13 Mw 6 earthquakes (yellow stars) along with Rapaki and Purau sites.

Fig. 7. Each panel shows seismic data from LPCC (A and B), D13C (C), D15C (D), and GODS (E) stations. Panels A and B compare ground motion, respectively, for 2011-02-22 Mw 6.2 and 2011-06-13 Mw 6 earthquakes at LPCC station. The left column shows east and north components of the velocity seismogram (blue line) and their respective envelopes (red dashed-line). The particle velocity hodogram (middle column, green line) was determined for a time window ± 5 s (shaded region in the left column) around the peak (red circle) of the east component envelope. The strike of the rock face (black short line segments) and the direction of the free face (red arrows) for sites PD1, PD2, PD3, PD4, and RAP are also illustrated. The particle motion hodogram (grey line) is presented in the right column, where green, yellow, and red segments represent, respectively, time points at which east component, north component, or both components exceed an acceleration of 0.3g. Note that scale of figure axes varies by station particularly for ground motion.

Fig. 8. **(A)** Rockfall size distribution as a proportion of boulders less than a given size plotted in log-space for CES and pre-CES rockfalls at Rapaki. **(B)** Rockfall frequency/size distribution for CES and pre-CES rockfalls at Rapaki. **(C)** Rockfall size distribution as a proportion of boulders less than a given size plotted in log-space for CES and pre-CES rockfalls at Purau. **(D)** Rockfall frequency/size distribution for CES and pre-CES rockfalls at Purau. **(E)** Comparison of boulder size distributions for CES and pre-CES VB and CL rockfalls at Rapaki study site. **(F)** Comparison of boulder size distributions for CES and pre-CES VB and CL rockfalls at Purau.

Fig. 9. **(A)** Frequency ratio versus volume ratio for pre-CES and CES rockfall boulders. **(B)** Frequency-runout distributions for Rapaki pre-CES and CES boulders. Both power law (without extrapolated data) and exponential (all data) fits are shown for the prehistoric boulder data set. A poor exponential fit is shown for CES rockfalls. **(C)** Plot of travel distance on talus slope (Lt) versus height on talus slope (Ht) with fitted polynomial regression lines for pre-CES and CES rockfalls at Rapaki. **(D)** Plot of Lt versus Ht with fitted linear, log, and polynomial regression lines for pre-CES and CES rockfalls at Purau. Four (4) separated domains (here D1-D4) are defined at Purau to evaluate the shadow angle method. **(E)** Plot of rockfall size (m^3) versus tangent of the shadow angle (Ht/Lt) for Rapaki rockfalls. No tendency of the data is evident. **(F)** Plot of rockfall size (m^3) versus tangent of the shadow

angle (Ht/Lt) for Purau rockfalls. The tendency for the domain data sets is poor. Values of correlation coefficients are below 0.3.

Fig. 10. **(A)** RAMMS_1 shows deposited rocks for simulated CES boulders. Mapped CES boulders (red circles) are shown for comparison. Boulder densities of 2500 kg/m^3 and 3000 kg/m^3 are used for VB and CL boulders, respectively. **(B)** Final resting locations for RAMMS_2 rockfalls. RAMMS_2 assumes prehistoric rockfall conditions (i.e. forested hillslope). Mapped prehistoric rockfalls are depicted (yellow circles) for comparison. An increase in forest density to 10,000 kg/s generates the best fit with maximum runout distance (see white dashed line) for mapped prehistoric boulders. **(C)** Final resting locations for RAMMS_3 boulders. RAMMS_3 assumes modern hillslope conditions (i.e. deforested hillslope). Note the increased maximum runout distance for RAMMS_3 boulders compared with RAMMS_2 and the potential future rockfall hazard to development sites S1 and S2.

Fig. 11. RAMMS simulated rockfall boulders showing differences in spatial distribution between VB (mostly equant shaped) and CL (predominantly elongate and flat shaped) boulder morphologies at Purau. All simulated boulders assume a volume of 1.0 m^3. **(A)** Spatial distribution of simulated VB boulders at Purau CES-7 location. Note the high relative percentage of simulated boulders deposited at the base of the hillslope (~500-600 meters from source rock). **(B)** Spatial distribution of simulated CL boulders at CES-7 location. Note the higher relative percentage of rockfall boulders deposited near the source rock (within ~100 meters from source rock). The simulation highlights the strong influence of boulder shape on runout distance.

Fig. 12. CES and pre-CES rockfall boulders within drainage valleys at Rapaki **(A, C)** and Purau **(B, D, E, F)** study locations. Drainage valleys contain a high amount of pre-CES rockfall boulders, which impacts the trajectory/path of CES rockfalls and reduces or stops runout distance.

Fig. 13. Velocity spectra for the 2011-06-13 Mw 6 earthquake recorded at station D13C. No path corrections are applied.

Table Captions

Table 1. Volumetric comparison of pre-CES and CES rockfall boulders (for volume ≥1.0 m^3) at Rapaki and Purau study sites.

Table 2. Comparison of boulder size statistics for Rapaki and Purau VB and CL pre-CES and CES rockfall boulders (for volume ≥1.0 m^3).

Table 3. (A) Comparison of frequency (n) and volume (m^3) ratios for pre-CES and CES rockfall boulders at the Rapaki and Purau study sites. **(B)** Comparison of VB/CL frequency (n) and volume (m^3) ratios for pre-CES and CES rockfall boulders at the Rapaki and Purau study sites.

Table 4. Average and maximum runout distances for pre-CES and CES rockfall boulders (for volume ≥1.0 m^3) at Rapaki and Purau study sites.

Appendix 1

Fig. A1. The total number of boulders with volume ≥ 0.1 m^3 were taken at runout distances of 1-10 m (yellow polygon 1), 30-40 m (yellow polygon 2), 60-70 m (yellow polygon 3), and 100-110 m (yellow polygon 4) from the volcanic source rock to estimate the total number of boulders in areas near the source cliff where conditions were unsafe for continuous mapping. The number of boulders in areas 'b' and 'c' were reduced by factors of 2 and 3, respectively, based upon field observations. The total number of rockfall boulders for the area (yellow dashed line) was normalized to a boulder size of 1.0 m^3 using a power law frequency-size distribution (as determined at the Rapaki study location).

Fig. A2. Conceptual diagram of hillslope illustrating the source rock cliff and the talus slope. The reach angle (A) and shadow angle (B) are shown. Sketch modified from Hungr (1993), Wieczorek et al. (2008) and Copons et al. (2009).

Fig. A3. Final resting locations for RAMMS_2 rockfalls assuming uniform forest density increase of 10,000 kg/s.

Appendix 2

Table A1. Friction parameters chosen for each terrain type in RAMMS.

Fig. A1. Polygon shapefiles for runout terrain types.

Fig. A2. Polyline shapefiles for RAMMS_1 rockfall source areas.

Fig. A3. Polyline shapefiles for RAMMS_2 and RAMMS_3 rockfall source areas.

Fig. A4 Polygon shapefiles for forest density.

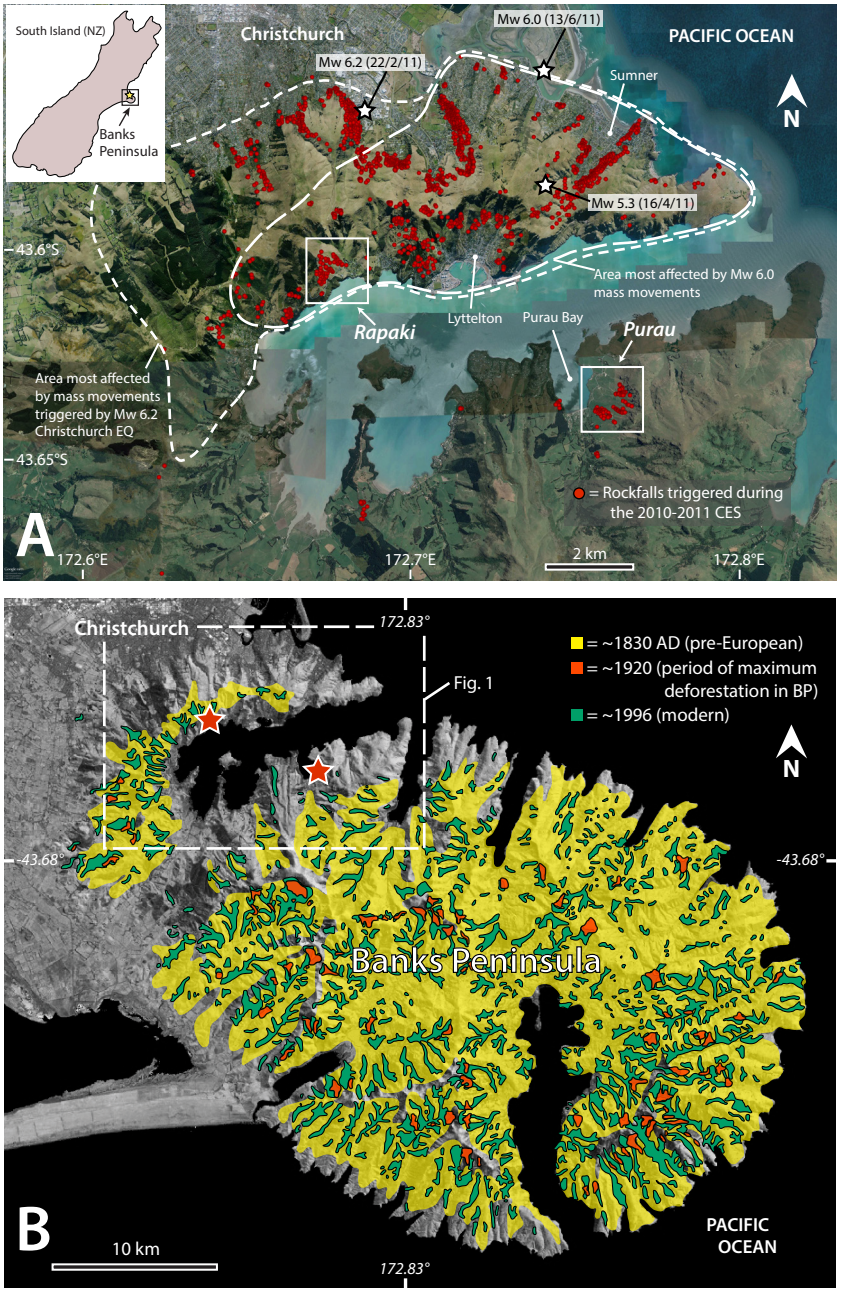
South Island (NZ)
Banks Peninsula
Christchurch
Mw 6.0 (13/6/11)
PACIFIC OCEAN
Mw 6.2 (22/2/11)
Sumner
N
Mw 5.3 (16/4/11)
43.6°S
Area most affected by Mw 6.0 mass movements
Rapaki
Lyttelton
Purau Bay
Purau
Area most affected by mass movements triggered by Mw 6.2 Christchurch EQ
43.65°S
= Rockfalls triggered during the 2010-2011 CES
A
172.6°E
172.7°E
2 km
172.8°E
Christchurch
172.83°
Fig. 1
= ~1830 AD (pre-European)
= ~1920 (period of maximum deforestation in BP)
= ~1996 (modern)
N
-43.68°
-43.68°
Banks Peninsula
B
10 km
PACIFIC OCEAN
172.83°

Figure 1

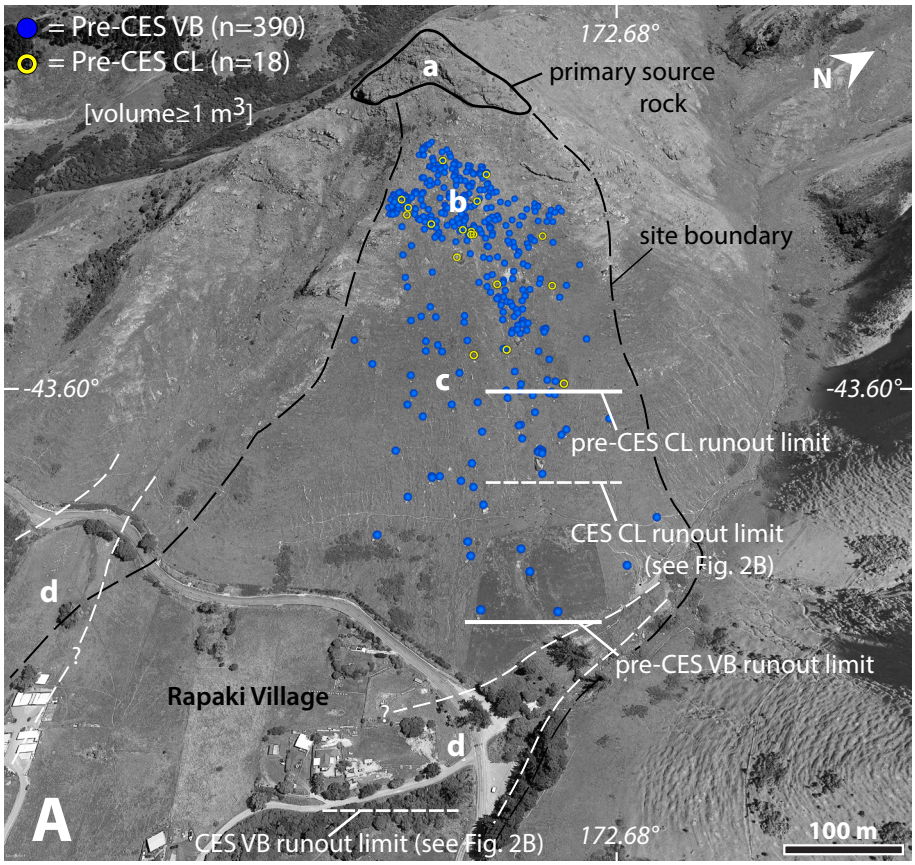
= Pre-CES VB (n=390)
= Pre-CES CL (n=18)
[volume≥1 m3]
172.68°
primary source rock
N
a
b
site boundary
-43.60°
c
-43.60°
pre-CES CL runout limit
CES CL runout limit (see Fig. 2B)
d
pre-CES VB runout limit
Rapaki Village
d
A
CES VB runout limit (see Fig. 2B)
172.68°
100 m

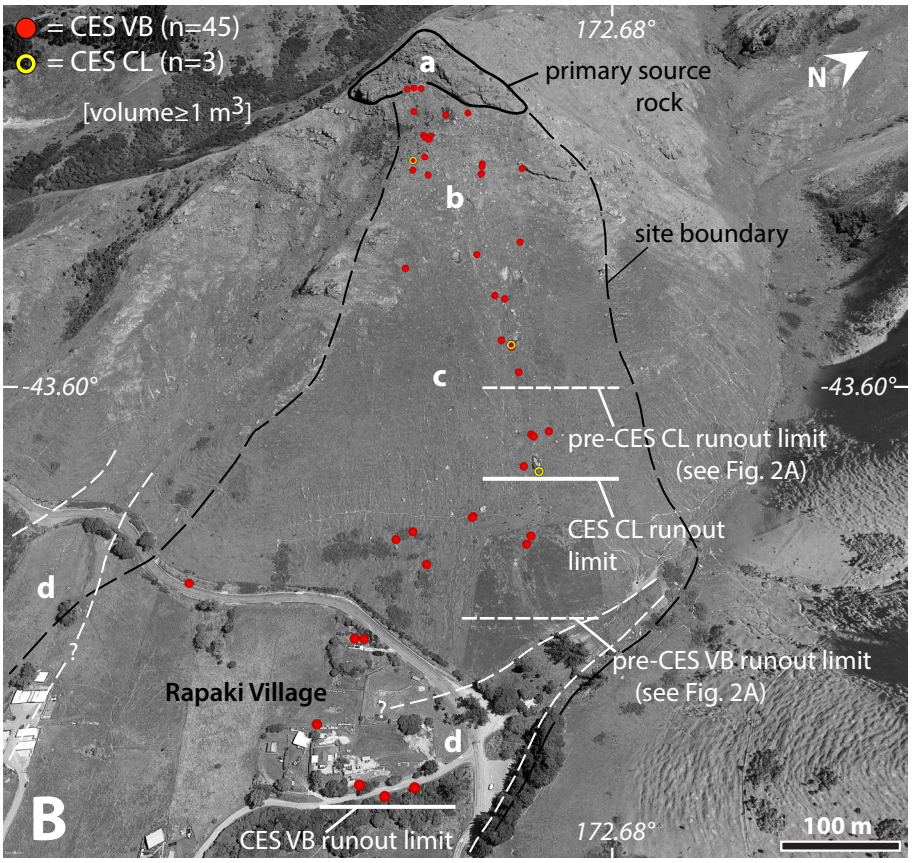
= CES VB (n=45)
= CES CL (n=3)
[volume≥1 m3]
172.68°
primary source rock
N
a
b
site boundary
-43.60°
c
-43.60°
pre-CES CL runout limit (see Fig. 2A)
CES CL runout limit
d
pre-CES VB runout limit (see Fig. 2A)
Rapaki Village
d
B
CES VB runout limit
172.68°
100 m

Figure 2

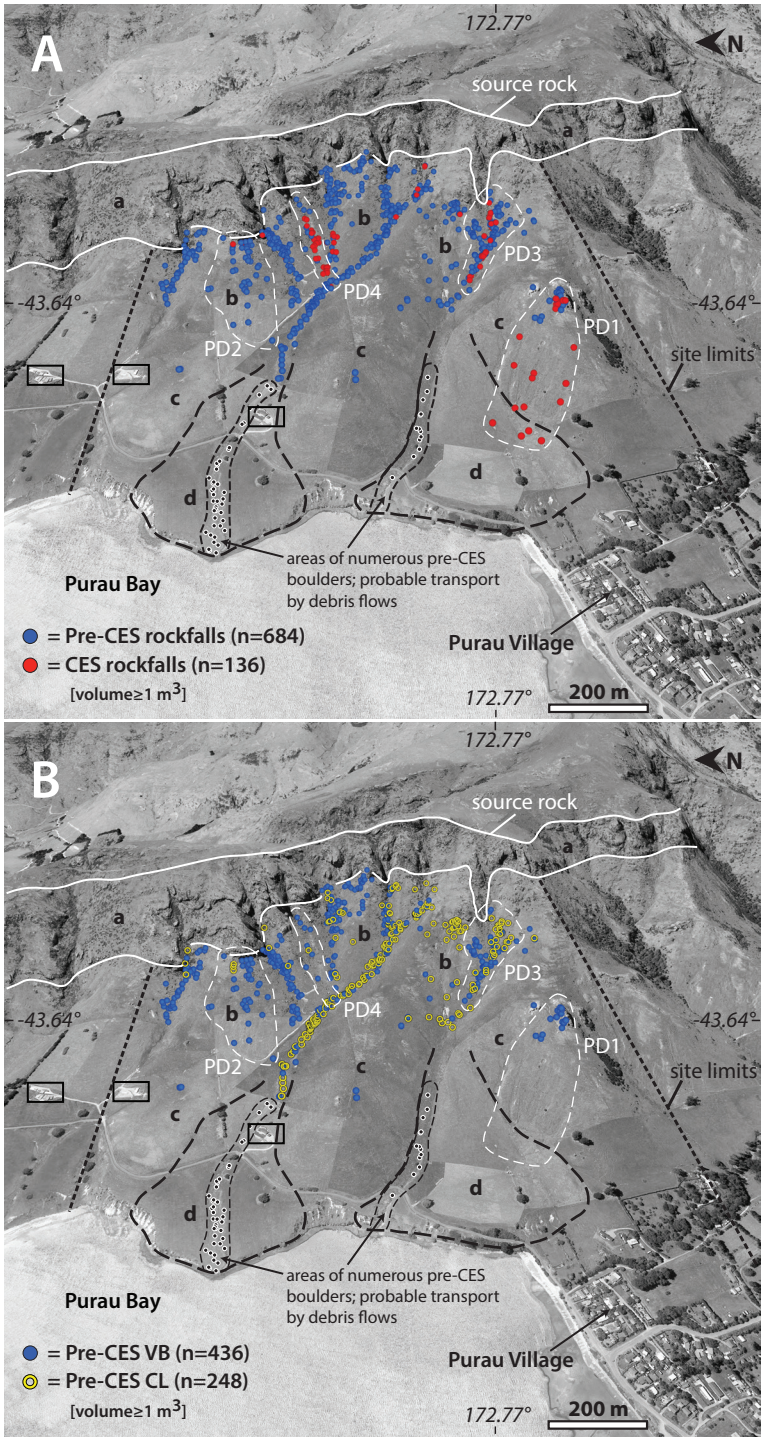
A
172.77°
N
source rock
a
b
PD3
PD4
-43.64°
PD2
c
PD1
site limits
d
areas of numerous pre-CES boulders; probable transport by debris flows
Purau Bay
Purau Village
= Pre-CES rockfalls (n=684)
= CES rockfalls (n=136)
[volume≥1 m3]
200 m

B
172.77°
N
source rock
a
b
PD3
PD4
-43.64°
PD2
c
PD1
site limits
d
areas of numerous pre-CES boulders; probable transport by debris flows
Purau Bay
Purau Village
= Pre-CES VB (n=436)
= Pre-CES CL (n=248)
[volume≥1 m3]
200 m

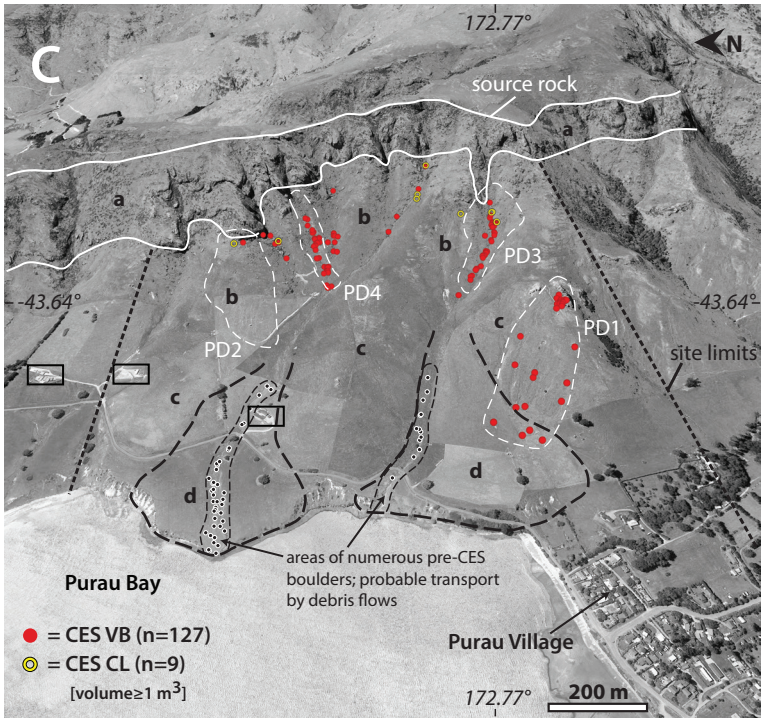
C
172.77°
N
source rock
a
b
PD3
PD4
-43.64°
PD2
c
PD1
site limits
d
areas of numerous pre-CES boulders; probable transport by debris flows
Purau Bay
Purau Village
= CES VB (n=127)
= CES CL (n=9)
[volume≥1 m3]
200 m

Figure 3

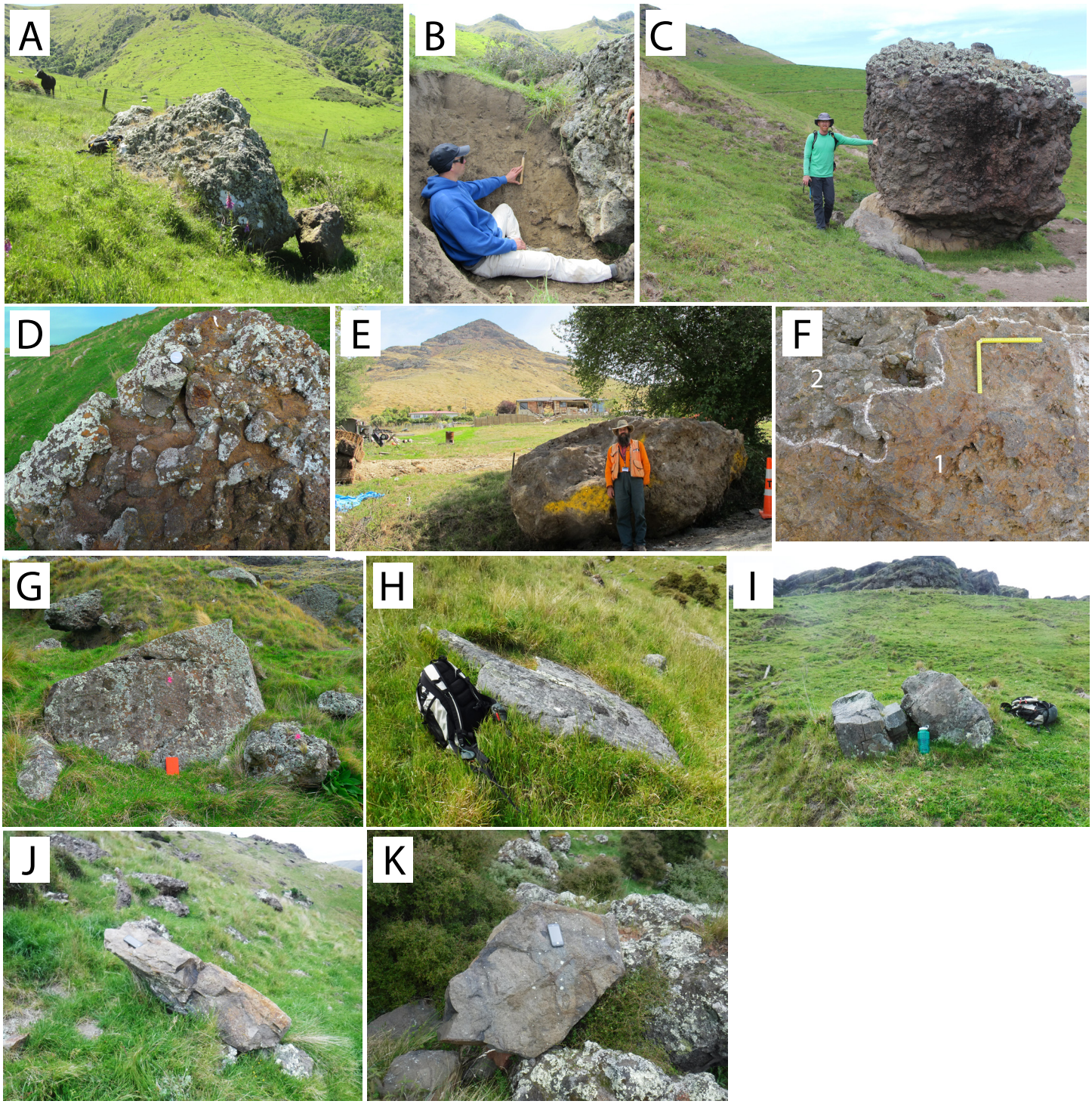

Figure 4

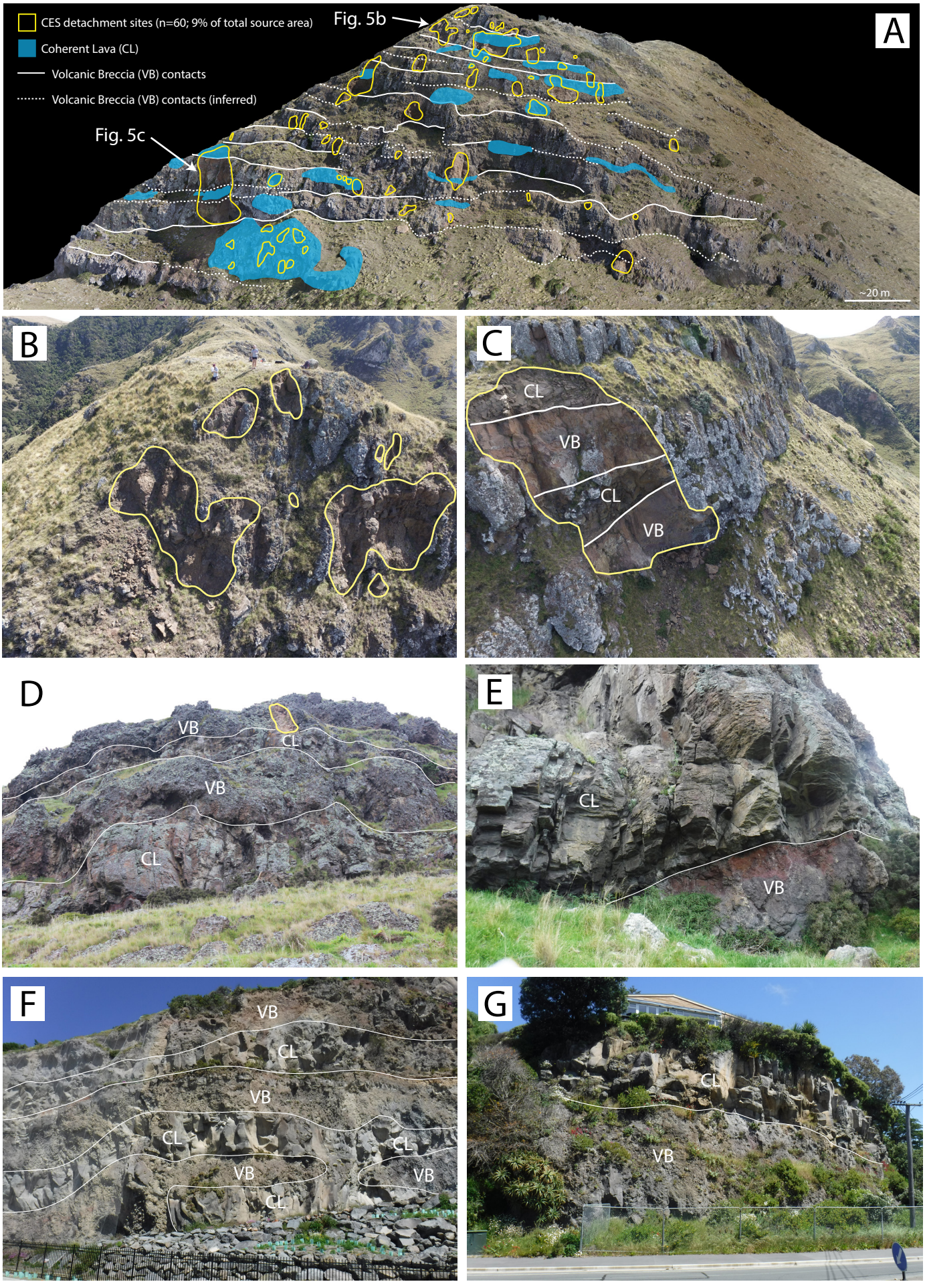
CES detachment sites (n=60; 9% of total source area)
Coherent Lava (CL)
Volcanic Breccia (VB) contacts
Volcanic Breccia (VB) contacts (inferred)
Fig. 5b
Fig. 5c
A
~20 m
B
C
CL
VB
CL
VB
D
VB
CL
VB
CL
E
CL
VB
F
VB
CL
VB
CL
CL
VB
VB
CL
G
CL
VB

Figure 5

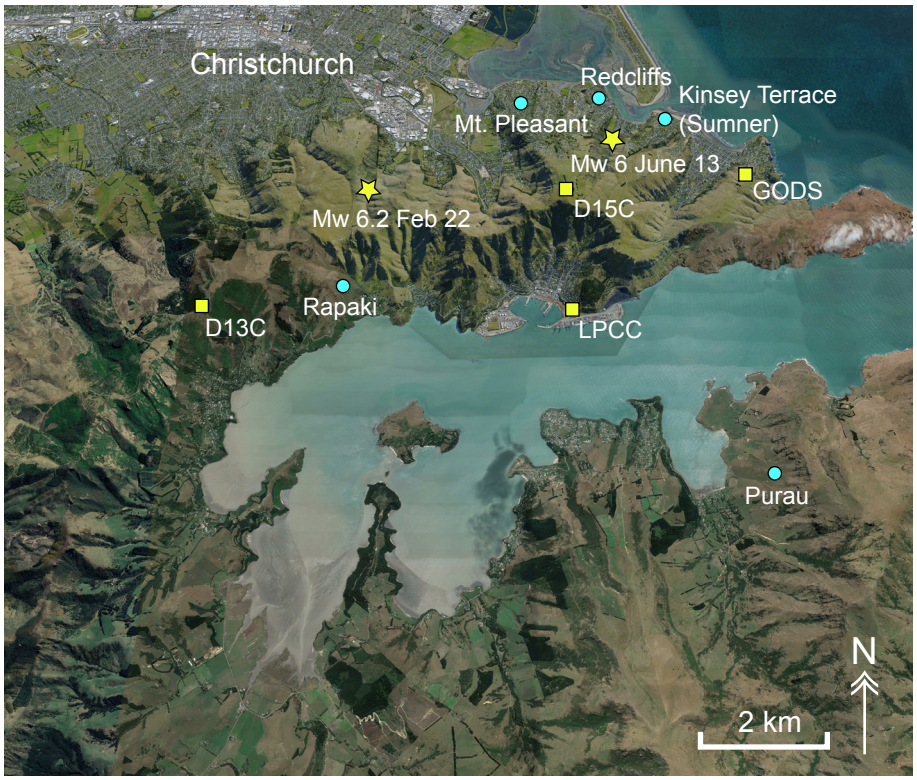
Christchurch
Redcliffs
Kinsey Terrace
(Sumner)
Mt. Pleasant
Mw 6 June 13
GODS
D15C
Mw 6.2 Feb 22
Rapaki
D13C
LPCC
Purau
N
2 km

Figure 6

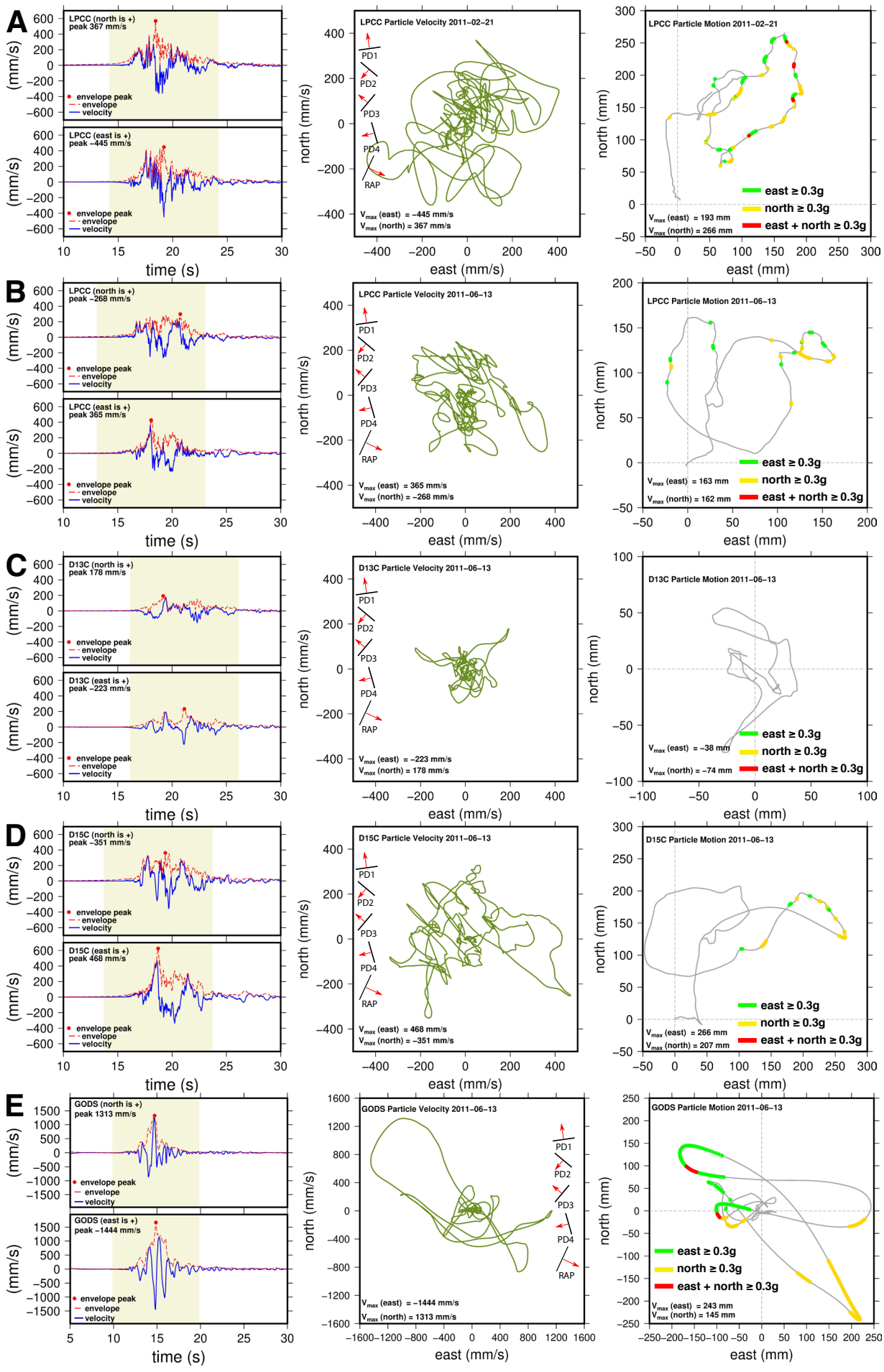
A
LPCC (north is +)
peak 367 mm/s
LPCC (east is +)
peak −445 mm/s
envelope peak
envelope
velocity
(mm/s)
time (s)
LPCC Particle Velocity 2011−02−21
PD1
PD2
PD3
PD4
RAP
Vmax (east) = −445 mm/s
Vmax (north) = 367 mm/s
north (mm/s)
east (mm/s)
LPCC Particle Motion 2011−02−21
Vmax (east) = 193 mm
Vmax (north) = 266 mm
east ≥ 0.3g
north ≥ 0.3g
east + north ≥ 0.3g
north (mm)
east (mm)
B
LPCC (north is +)
peak −268 mm/s
LPCC (east is +)
peak 365 mm/s
LPCC Particle Velocity 2011−06−13
Vmax (east) = 365 mm/s
Vmax (north) = −268 mm/s
LPCC Particle Motion 2011−06−13
Vmax (east) = 163 mm
Vmax (north) = 162 mm
C
D13C (north is +)
peak 178 mm/s
D13C (east is +)
peak −223 mm/s
D13C Particle Velocity 2011−06−13
Vmax (east) = −223 mm/s
Vmax (north) = 178 mm/s
D13C Particle Motion 2011−06−13
Vmax (east) = −38 mm
Vmax (north) = −74 mm
D
D15C (north is +)
peak −351 mm/s
D15C (east is +)
peak 468 mm/s
D15C Particle Velocity 2011−06−13
Vmax (east) = 468 mm/s
Vmax (north) = −351 mm/s
D15C Particle Motion 2011−06−13
Vmax (east) = 266 mm
Vmax (north) = 207 mm
E
GODS (north is +)
peak 1313 mm/s
GODS (east is +)
peak −1444 mm/s
GODS Particle Velocity 2011−06−13
Vmax (east) = −1444 mm/s
Vmax (north) = 1313 mm/s
GODS Particle Motion 2011−06−13
Vmax (east) = 243 mm
Vmax (north) = 145 mm

Figure 7

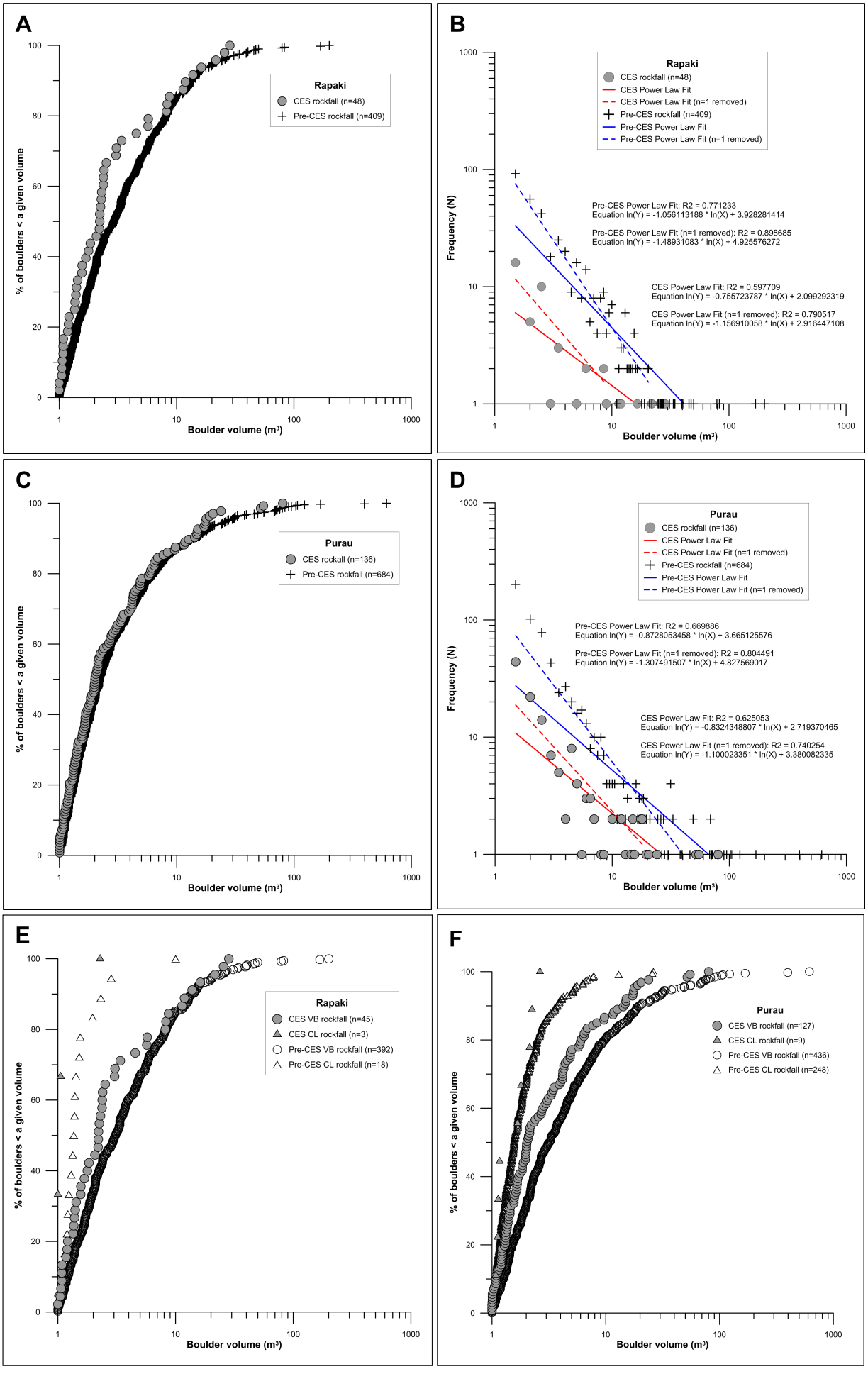
A
% of boulders < a given volume
Boulder volume (m³)
Rapaki
CES rockfall (n=48)
Pre-CES rockfall (n=409)
B
Frequency (N)
Boulder volume (m³)
Rapaki
CES rockfall (n=48)
CES Power Law Fit
CES Power Law Fit (n=1 removed)
Pre-CES rockfall (n=409)
Pre-CES Power Law Fit
Pre-CES Power Law Fit (n=1 removed)
Pre-CES Power Law Fit: R2 = 0.771233
Equation ln(Y) = -1.056113188 * ln(X) + 3.928281414
Pre-CES Power Law Fit (n=1 removed): R2 = 0.898685
Equation ln(Y) = -1.48931083 * ln(X) + 4.925576272
CES Power Law Fit: R2 = 0.597709
Equation ln(Y) = -0.755723787 * ln(X) + 2.099292319
CES Power Law Fit (n=1 removed): R2 = 0.790517
Equation ln(Y) = -1.156910058 * ln(X) + 2.916447108
C
% of boulders < a given volume
Boulder volume (m³)
Purau
CES rockall (n=136)
Pre-CES rockfall (n=684)
D
Frequency (N)
Boulder volume (m³)
Purau
CES rockfall (n=136)
CES Power Law Fit
CES Power Law Fit (n=1 removed)
Pre-CES rockfall (n=684)
Pre-CES Power Law Fit
Pre-CES Power Law Fit (n=1 removed)
Pre-CES Power Law Fit: R2 = 0.669886
Equation ln(Y) = -0.8728053458 * ln(X) + 3.665125576
Pre-CES Power Law Fit (n=1 removed): R2 = 0.804491
Equation ln(Y) = -1.307491507 * ln(X) + 4.827569017
CES Power Law Fit: R2 = 0.625053
Equation ln(Y) = -0.8324348807 * ln(X) + 2.719370465
CES Power Law Fit (n=1 removed): R2 = 0.740254
Equation ln(Y) = -1.100023351 * ln(X) + 3.380082335
E
% of boulders < a given volume
Boulder volume (m³)
Rapaki
CES VB rockfall (n=45)
CES CL rockfall (n=3)
Pre-CES VB rockfall (n=392)
Pre-CES CL rockfall (n=18)
F
% of boulders < a given volume
Boulder volume (m³)
Purau
CES VB rockfall (n=127)
CES CL rockfall (n=9)
Pre-CES VB rockfall (n=436)
Pre-CES CL rockfall (n=248)

Figure 8

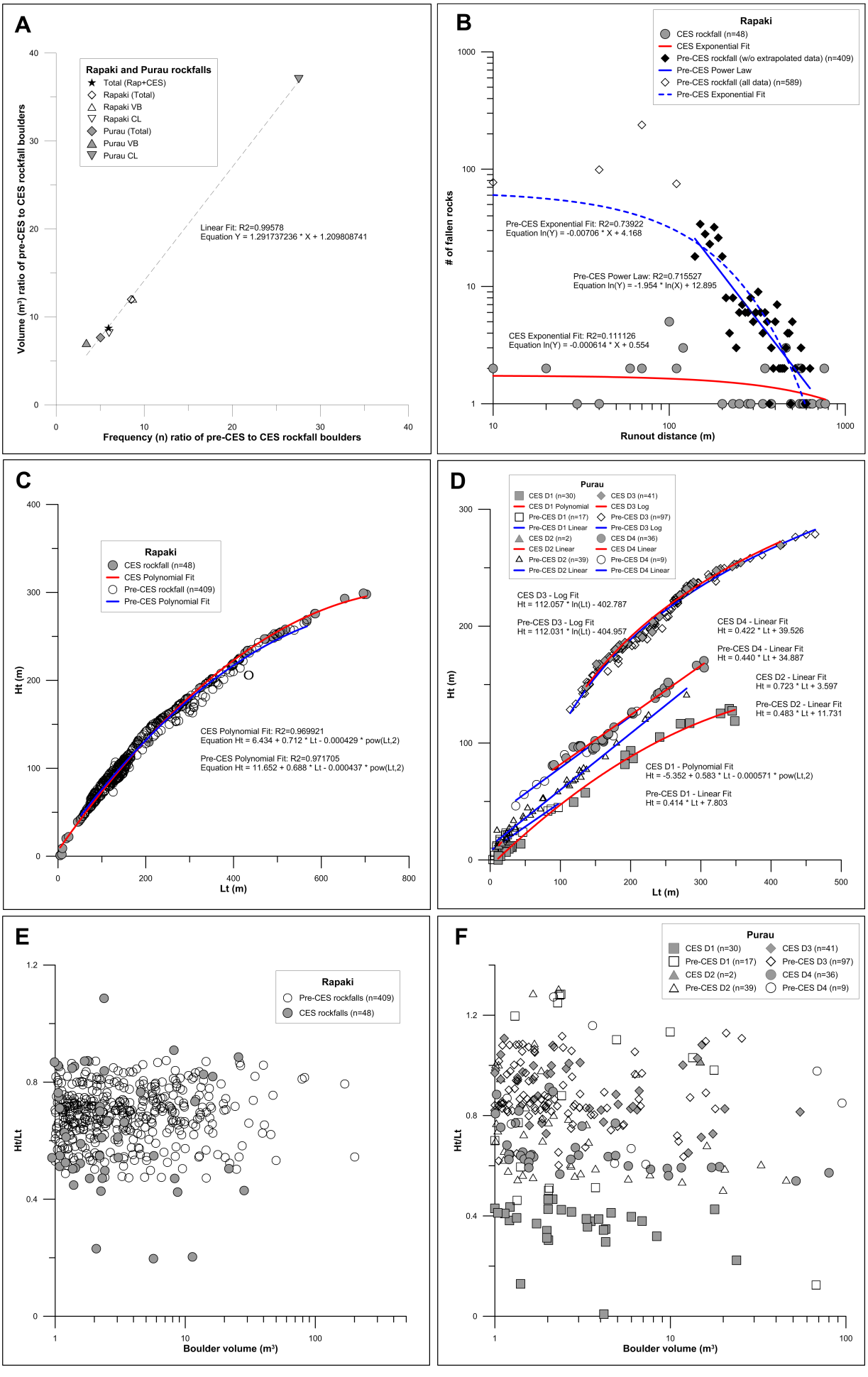
A
Rapaki and Purau rockfalls
Total (Rap+CES)
Rapaki (Total)
Rapaki VB
Rapaki CL
Purau (Total)
Purau VB
Purau CL
Linear Fit: R2=0.99578
Equation Y = 1.291737236 * X + 1.209808741
Volume (m³) ratio of pre-CES to CES rockfall boulders
Frequency (n) ratio of pre-CES to CES rockfall boulders
B
Rapaki
CES rockfall (n=48)
CES Exponential Fit
Pre-CES rockfall (w/o extrapolated data) (n=409)
Pre-CES Power Law
Pre-CES rockfall (all data) (n=589)
Pre-CES Exponential Fit
Pre-CES Exponential Fit: R2=0.73922
Equation ln(Y) = -0.00706 * X + 4.168
Pre-CES Power Law: R2=0.715527
Equation ln(Y) = -1.954 * ln(X) + 12.895
CES Exponential Fit: R2=0.111126
Equation ln(Y) = -0.000614 * X + 0.554
# of fallen rocks
Runout distance (m)
C
Rapaki
CES rockfall (n=48)
CES Polynomial Fit
Pre-CES rockfall (n=409)
Pre-CES Polynomial Fit
CES Polynomial Fit: R2=0.969921
Equation Ht = 6.434 + 0.712 * Lt - 0.000429 * pow(Lt,2)
Pre-CES Polynomial Fit: R2=0.971705
Equation Ht = 11.652 + 0.688 * Lt - 0.000437 * pow(Lt,2)
Ht (m)
Lt (m)
D
Purau
CES D1 (n=30)
CES D1 Polynomial
Pre-CES D1 (n=17)
Pre-CES D1 Linear
CES D2 (n=2)
CES D2 Linear
Pre-CES D2 (n=39)
Pre-CES D2 Linear
CES D3 (n=41)
CES D3 Log
Pre-CES D3 (n=97)
Pre-CES D3 Log
CES D4 (n=36)
CES D4 Linear
Pre-CES D4 (n=9)
Pre-CES D4 Linear
CES D3 - Log Fit
Ht = 112.057 * ln(Lt) - 402.787
Pre-CES D3 - Log Fit
Ht = 112.031 * ln(Lt) - 404.957
CES D4 - Linear Fit
Ht = 0.422 * Lt + 39.526
Pre-CES D4 - Linear Fit
Ht = 0.440 * Lt + 34.887
CES D2 - Linear Fit
Ht = 0.723 * Lt + 3.597
Pre-CES D2 - Linear Fit
Ht = 0.483 * Lt + 11.731
CES D1 - Polynomial Fit
Ht = -5.352 + 0.583 * Lt - 0.000571 * pow(Lt,2)
Pre-CES D1 - Linear Fit
Ht = 0.414 * Lt + 7.803
Ht (m)
Lt (m)
E
Rapaki
Pre-CES rockfalls (n=409)
CES rockfalls (n=48)
Ht/Lt
Boulder volume (m³)
F
Purau
CES D1 (n=30)
Pre-CES D1 (n=17)
CES D2 (n=2)
Pre-CES D2 (n=39)
CES D3 (n=41)
Pre-CES D3 (n=97)
CES D4 (n=36)
Pre-CES D4 (n=9)
Ht/Lt
Boulder volume (m³)

Figure 9

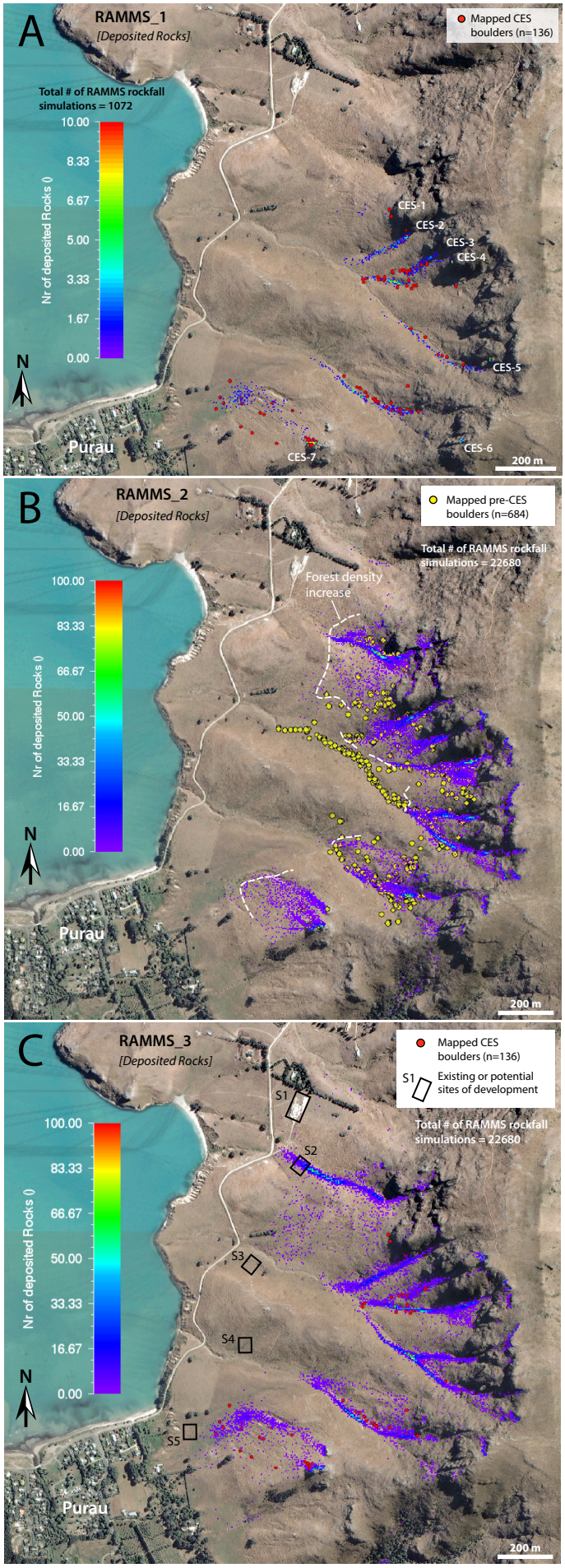
A
RAMMS_1
[Deposited Rocks]
Mapped CES boulders (n=136)
Total # of RAMMS rockfall simulations = 1072
Nr of deposited Rocks ()
10.00
8.33
6.67
5.00
3.33
1.67
0.00
CES-1
CES-2
CES-3
CES-4
CES-5
CES-6
CES-7
N
Purau
200 m
B
RAMMS_2
[Deposited Rocks]
Mapped pre-CES boulders (n=684)
Total # of RAMMS rockfall simulations = 22680
Forest density increase
100.00
83.33
66.67
50.00
33.33
16.67
0.00
Nr of deposited Rocks ()
N
Purau
200 m
C
RAMMS_3
[Deposited Rocks]
Mapped CES boulders (n=136)
S1
Existing or potential sites of development
Total # of RAMMS rockfall simulations = 22680
S1
S2
S3
S4
S5
100.00
83.33
66.67
50.00
33.33
16.67
0.00
Nr of deposited Rocks ()
N
Purau
200 m

Figure 10

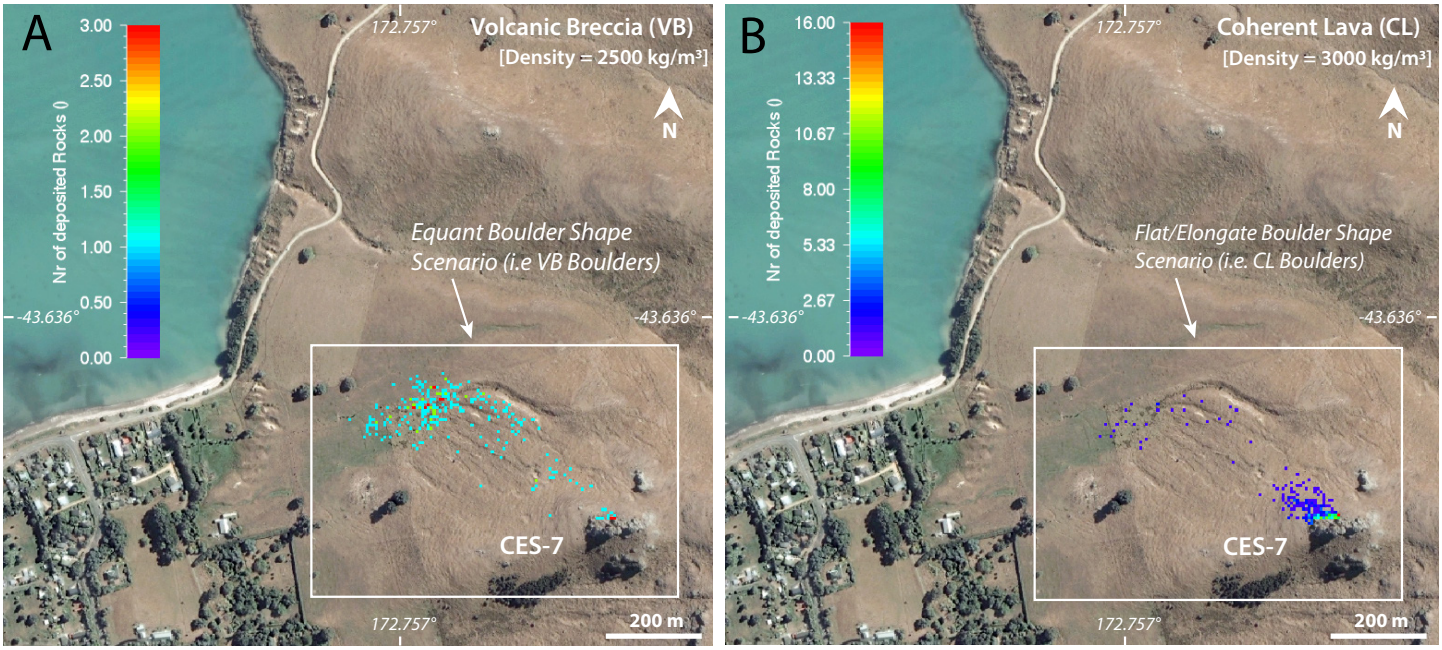
A
Volcanic Breccia (VB)
[Density = 2500 kg/m³]
Nr of deposited Rocks ()
3.00
2.50
2.00
1.50
1.00
0.50
0.00
172.757°
-43.636°
N
Equant Boulder Shape
Scenario (i.e VB Boulders)
CES-7
200 m
B
Coherent Lava (CL)
[Density = 3000 kg/m³]
16.00
13.33
10.67
8.00
5.33
2.67
0.00
Flat/Elongate Boulder Shape
Scenario (i.e. CL Boulders)

Figure 11

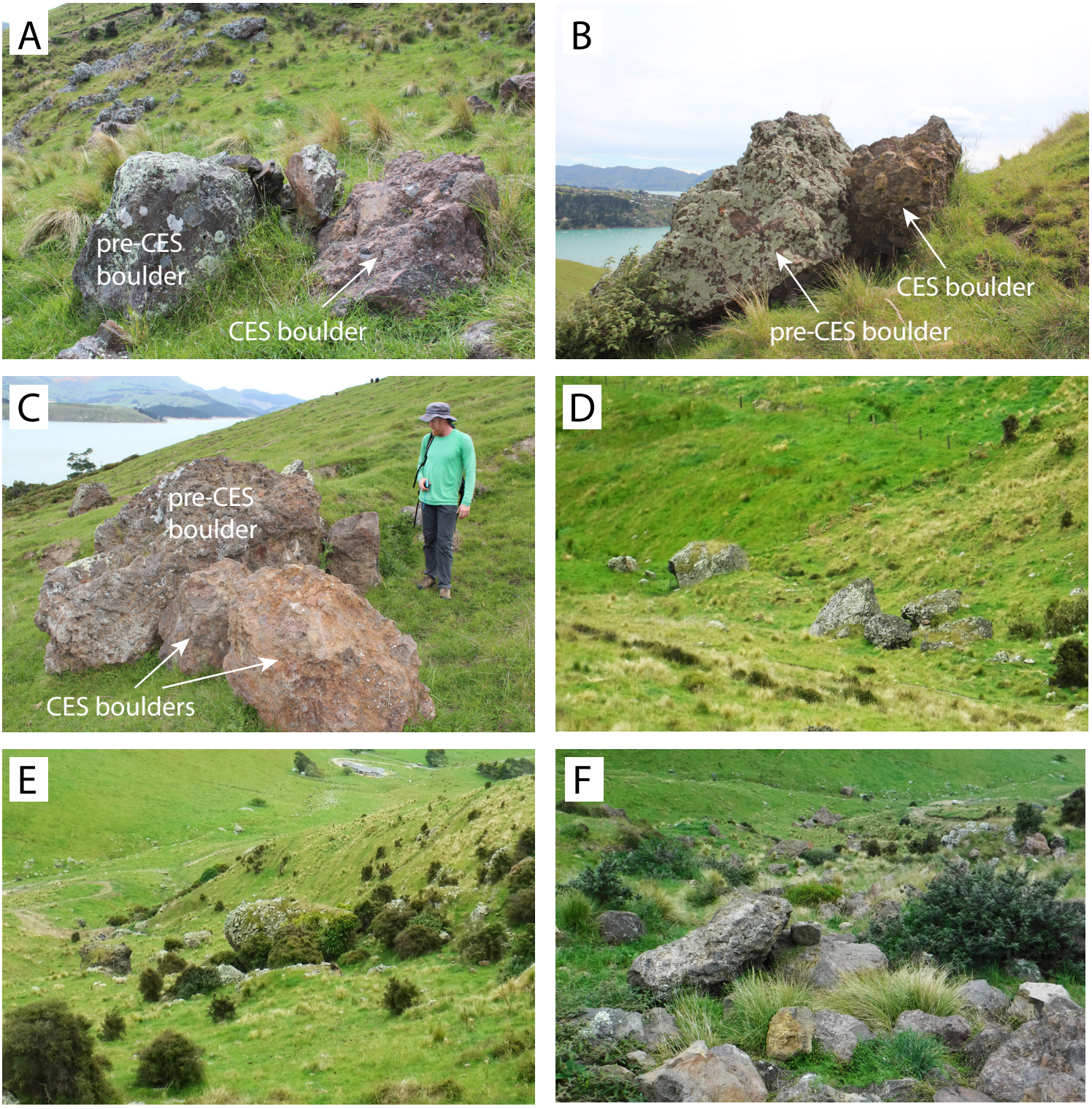
A
pre-CES boulder
CES boulder
B
CES boulder
pre-CES boulder
C
pre-CES boulder
CES boulders
D
E
F

Figure 12

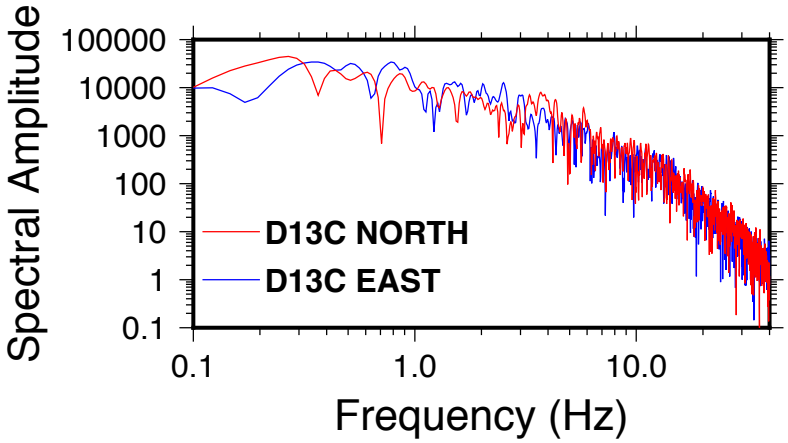
Spectral Amplitude
100000
10000
1000
100
10
1
0.1
D13C NORTH
D13C EAST
0.1
1.0
10.0
Frequency (Hz)

Figure 13

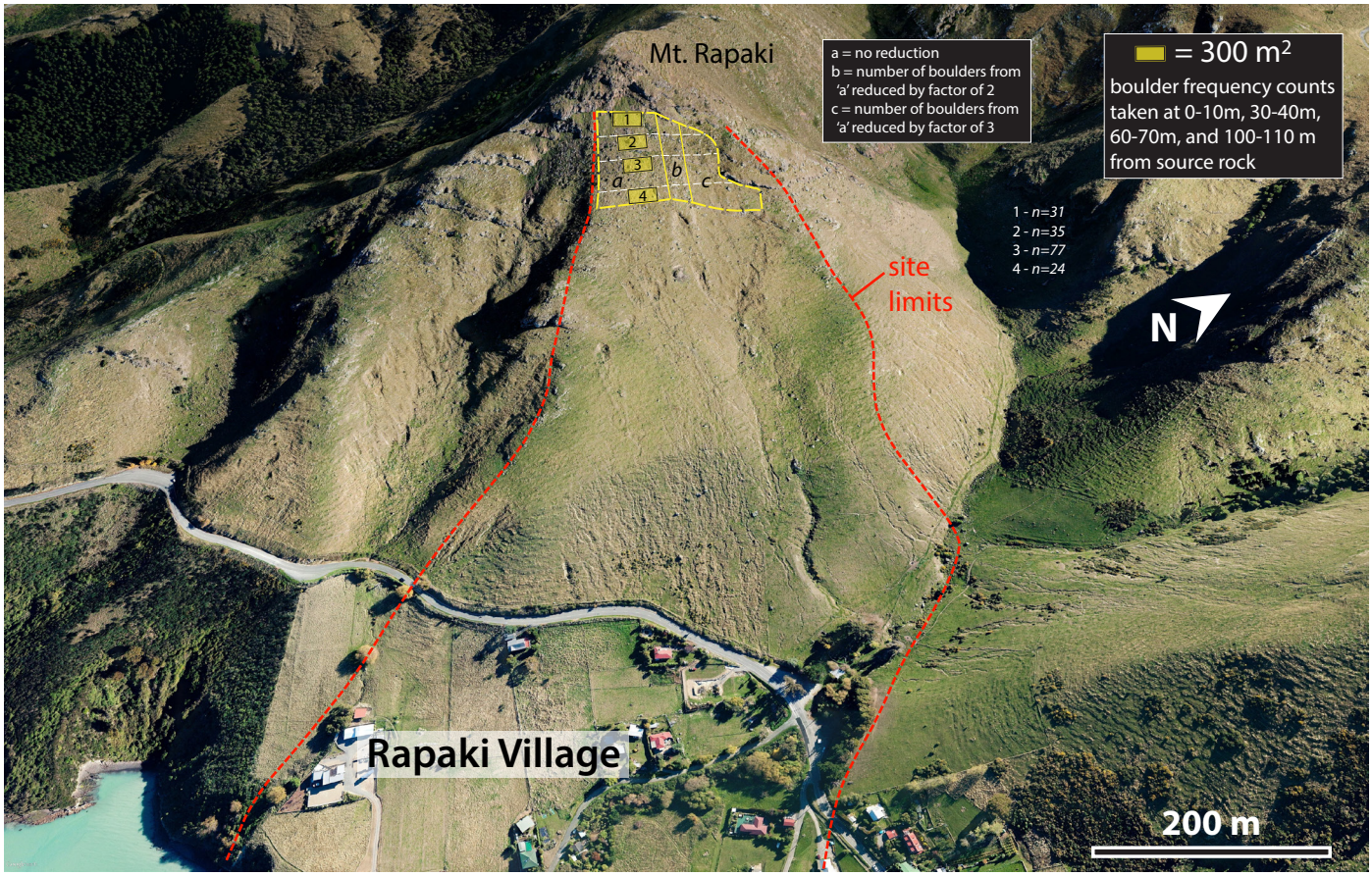

Appendix 1 - Figure A1

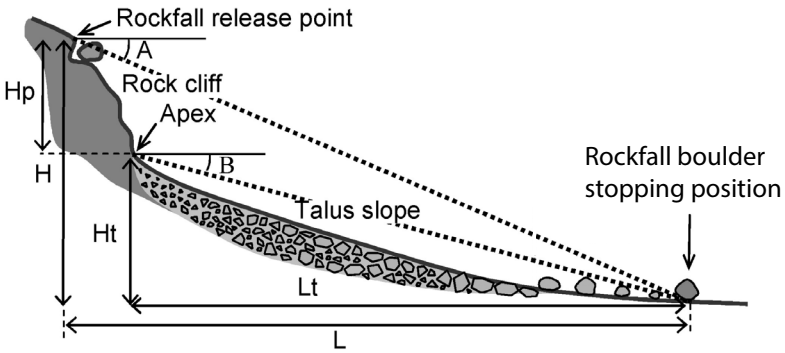

Appendix 1 - Figure A2

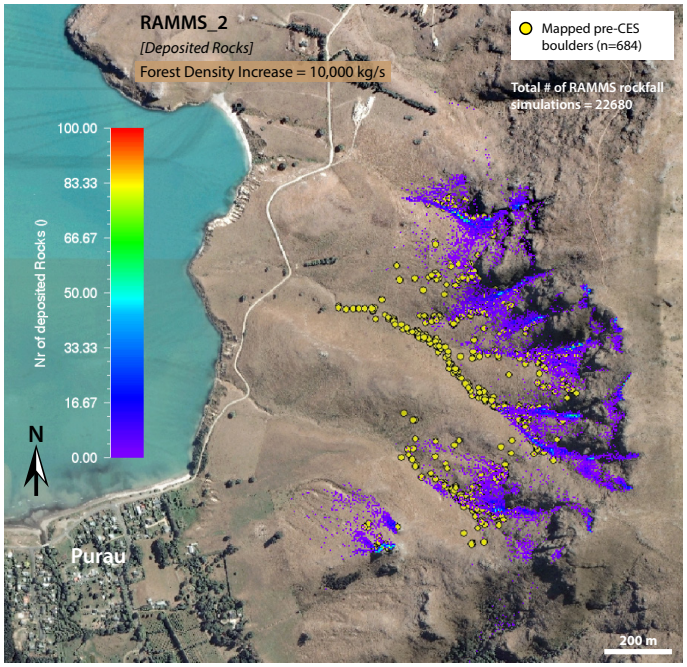

Appendix 1 - Figure A3

	μ_{min}	μ_{max}	ε	Drag layer coefficient	β	κ
Volcanic Rock	0.7	2.0	0	0.3	50	0.5
Loess and volcanic colluvium	0.45	2.0	0	0.5	30	0.6
Loess	0.3	2.0	0	0.5	30	0.5
Valley Terrain	0.2	2.0	0	0.9	25	0.5

Appendix 2_Table A1. Friction parameters chosen for each terrain type in RAMMS.

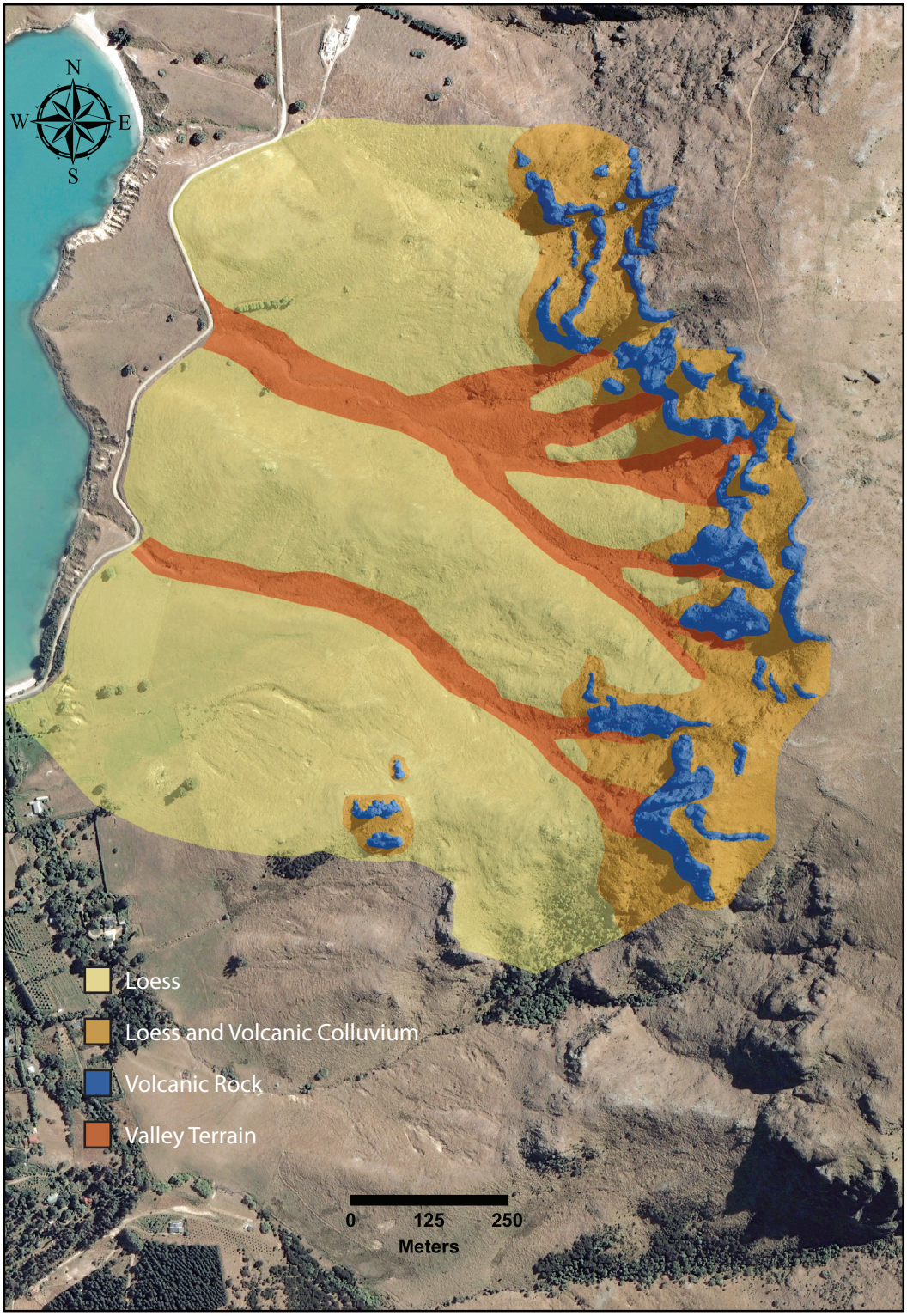

Appendix 2 - Figure A1

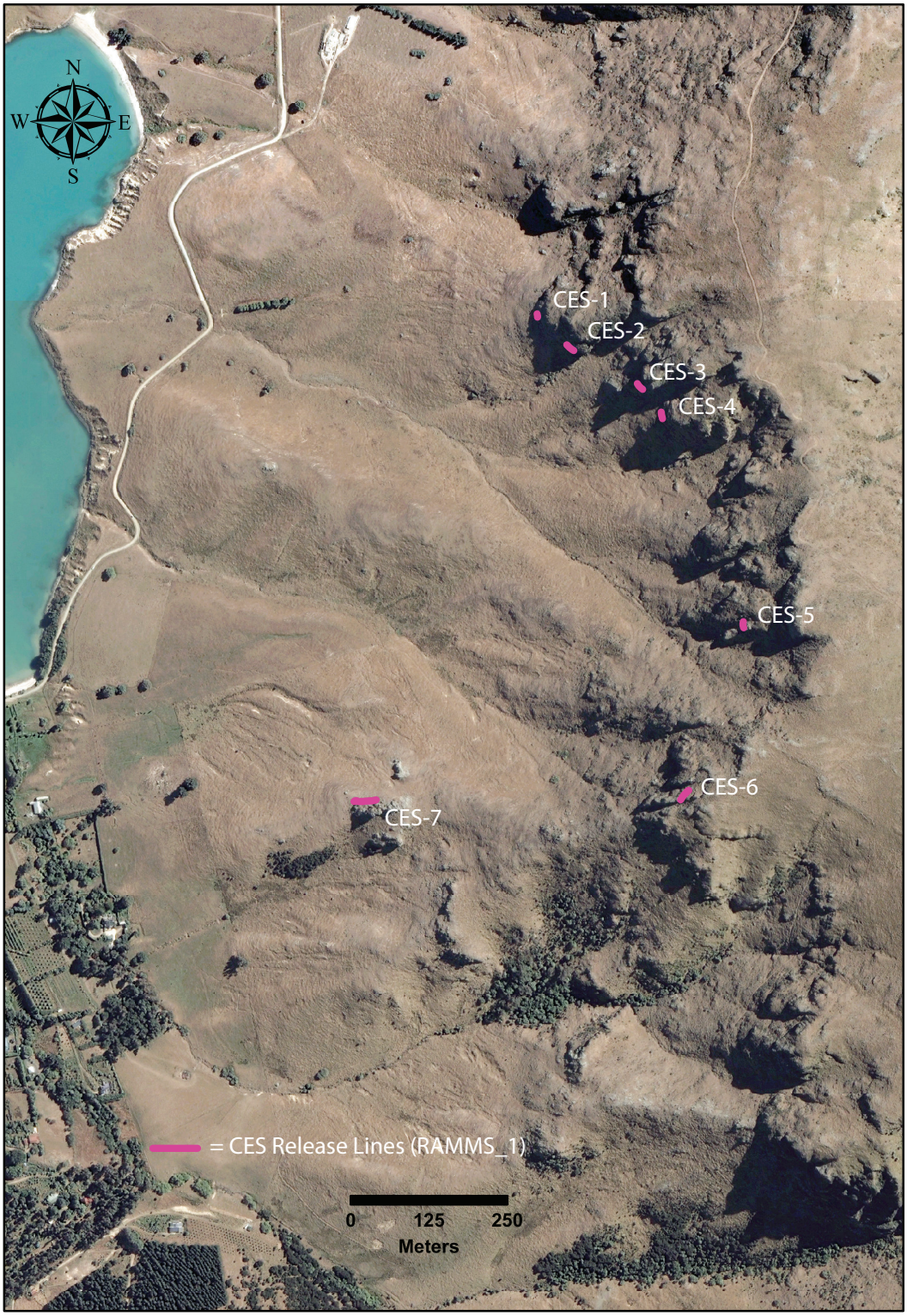

Appendix 2 - Figure A2

Appendix 2 - Figure A3

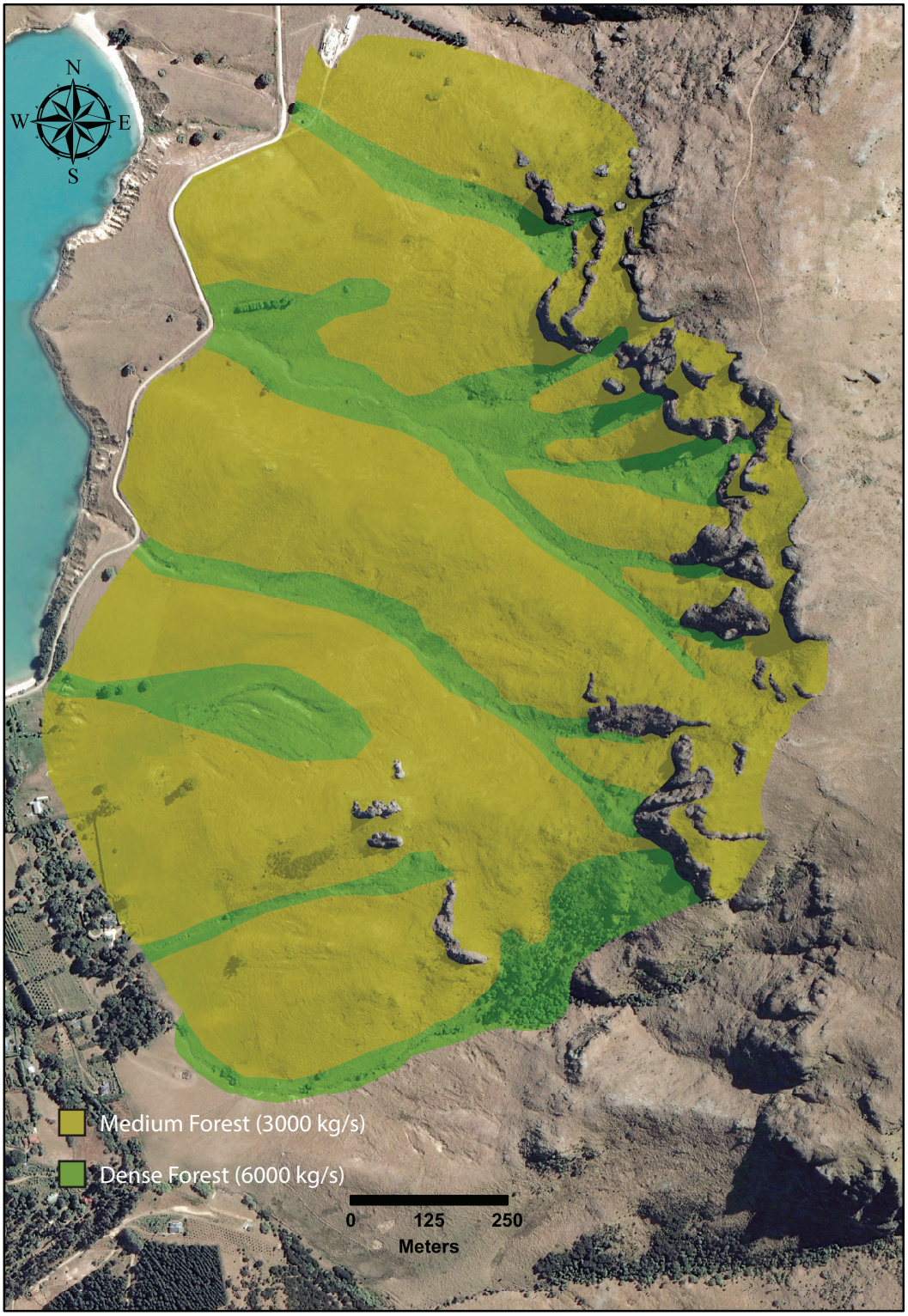

Appendix 2 - Figure A4